Biotribology 18 (2019) 100091

Contents lists available at ScienceDirect

Biotribology

journal homepage: www.elsevier.com/locate/biotri

Tribocorrosion of Polyethylene/Cobalt Contact Combined with Real-Time Fluorescence Assays on Living Macrophages: Development of A Multidisciplinary Biotribocorrosion Device

A. Impergre[a,b,*], A.M. Trunfio-Sfarghiu[b], C. Der-Loughian[a], L. Brizuela[c], S. Mebarek[c], B. Ter-Ovanessian[a], A. Bel-Brunon[b], Y. Berthier[b], B. Normand[a,*]

[a] Univ. Lyon, MATEIS, INSA de Lyon, UMR CNRS 5510, F-69621 Lyon, France
[b] Univ. Lyon, LaMCoS, INSA de Lyon, UMR CNRS 5259, F-69621 Lyon, France
[c] Univ. Lyon, ICBMS, INSA de Lyon, UMR CNRS 5246, F-69621 Lyon, France

ARTICLE INFO

Keywords:
Biotribocorrosion
CoCrMo
Fluorescence microscopy
Macrophage

ABSTRACT

The test conditions currently used in biotribocorrosion devices often differ greatly from the physiological conditions of joint replacements, contributing to discrepancies between the simulated and actual life span of joint replacements. In this study, a multidisciplinary biotribocorrosion device was developed based on the limitations of existing tribocorrosimeters. The set-up enables corrosion measurements to be simultaneously performed with real-time visualization of living cells using fluorescence microscopy under dynamic loads and movements. The device was configured to simulate the joint contact of ankle prostheses, and the wear of ultra-high-molecular-weight polyethylene/cobalt alloy (CoCrMo) implants surrounded by murine macrophages was tested. Various characterization techniques (non-contact optical profilometry, scanning and fluorescence electron microscopy and quantitative analyses of metal ions and pro-inflammatory cytokines) were combined in-depth multidisciplinary study. Two experimental conditions were used to promote the production of either polyethylene wear particles or metal ions. The first results indicated two distinct tribocorrosion mechanisms: 1) adhesive wear coupled with slow ionic depassivation of the cobalt alloy. The main degradation products were micrometric spherical polyethylene particles that seem to have little impact effect on the metabolic activity of the macrophages. 2) Ionic wear with the production of small, fibrillar polyethylene particles was observed. The production of metal ions, mainly chromium, was the predominant degradation process. The cytotoxicity of the chromium ions was evaluated based on the secretion of pro-inflammatory cytokines (prostaglandin E_2). Our findings indicate that simulated conditions that result in low mechanical wear but high ions release appear to be more harmful to cells.

1. Introduction

Extending the life of joint prostheses is one of the priorities of orthopaedic medicine and the science of biomedical materials. Depending on the clinical case, a revision prosthesis is required in 12%–17% of cases [1,2]. Prosthesis failure mainly results from the release and accumulation of degradation products, in the form of nanoparticles, microparticles and metal ions in the body [3,4]. Macrophages in the periprosthetic tissues phagocyte wear particles and become activated, releasing an array of proinflammatory cytokines, which leads to increased resorption of the adjacent bone [5–7]. *In vitro* and *in vivo* studies have demonstrated the toxicity of polyethylene particles [8–10]. Likewise, metal ions, such as Co^{2+}, Cr^{3+}, Cr^{6+}, are known to induce allergy, toxicity and necrosis in fibroblasts, osteoblasts, osteoclasts and macrophages [11–13]. The overall inflammatory response induced by all these degradation products result in aseptic loosening [14–16], which has been identified as one of the main causes of failure in total joint arthroplasty [17–19]. However, the mechanisms of the different reactions remain unclear and difficult to evaluate.

Joint simulators and tribometer devices are typically used to study mechanical wear and produce wear debris [20–24]. Tribometers are generally designed using a ball-on-plane or pin-on-plane configuration [25,26] consisting of a flat metal sample and an inert friction counter. Tribometers have been modified for operation in corrosive environments, to better reflect the aggressiveness of physiological fluids [27] and enable assessment of the synergistic interactions of wear and

* Corresponding author at : Univ. Lyon, MATEIS, INSA de Lyon, UMR CNRS 5510, Bâtiment Léonard de Vinci, 21 Avenue Jean Capelle, 69100 Villeurbanne, France.
E-mail addresses: amandine.impergre@insa-lyon.fr (A. Impergre), bernard.normand@insa-lyon.fr (B. Normand).

https://doi.org/10.1016/j.biotri.2019.100091
Received 31 October 2018; Received in revised form 24 March 2019; Accepted 25 March 2019
Available online 26 March 2019

corrosion, *i.e.*, tribocorrosion. Because different tribometer designs lead to the production of well-controlled wear debris in a wide variety of diluted saline solutions [28–33], it is critical that the conditions be kept as close as possible to the *in vivo* conditions to understand the actual levels of toxicity. Polyethylene wear debris retrieved from simulators are larger in size and shape than particles isolated from periprosthetic tissues [34]. In addition, it remains difficult to achieve similar concentrations of debris and ions as those found in periarticular tissues to simulate their cytotoxicity associated with osteolysis. Notably, the toxicity of degradation products *in vivo* may also result from the cumulative effect of different forms of wear debris and metal ions. The discrepancy between simulated and *in vivo* degradation products may also be related to the methodology used to produce the degradation products, which raises the question of the validity of current tribometers. The misunderstanding of joint contacts may stem from the poor representativeness of experimental conditions.

Previous studies have shown that the quantity of wear particles and metal ions vary depending on the generation method, resulting in considerable variation of their cytotoxicity [35,36]. The use of different friction couples have an impact on the nature and shape of the wear particles generated as well as the tribological behaviour. Therefore, the use of a hard material as counter-body to simulate wear of metal-on-polyethylene bearings is not appropriated. Only a few studies have focused on real tribocorrosion processes between a metal and polymer [37–39]. In addition, wear particles are not always generated from simulated friction, however commercially available nanoparticles and microparticles are also used to assess the cytotoxicity of wear particles from orthopaedic implants and prostheses. Similarly, the majority of studies have used salts ($CoCl_2$ or $CrCl_3$, Cr_6O_2, Cr_3O_4 or $K_2Cr_2O_7$) as a source of Co and Cr ions [40]. Thus, there are inherent limitations associated with the methods currently available to generate simulated degradation products.

Previous studies have provided evidences of the difference between the physico-chemical characteristics (shape, size, and ionic composition) of wear particles generated under different tribometer conditions and those of periprosthetic tissue samples obtained from revision surgery [41,42]. Disparities in the analysis result from variation in the isolation protocols. For polyethylene particles, three different isolation techniques (alkaline, acid, enzymatic) can be used. [43,44]. Isolation reagents may affect the particle morphology. For example, soluene can create cracks in the debris or even dissolve ultra-high-molecular-weight-polyethylene (UHMW-PE) particles [45]. The contamination of the biomaterial particles by cell debris or reagent particles is also a significant problem in the isolation of polyethylene particles [45]. The isolation process also includes a filtration step at different nanometre to micrometre pore sizes. The use of different filtration sizes causes a loss of nanometric wear debris and more importantly, the exclusion of metal ions produced by metallic dissolution [46]. Therefore using wear particles obtained from an isolation process and testing their biocompatibility should be avoided. Moreover, it is very difficult to collect and analyse degradation products when they are produced in a container separated from the one in which the cell culture occurs. Tribocorrosion devices have limitations in terms of simultaneous assessment of the degradation of biomaterials subjected to tribocorrosion and the cellular response. The lack of development of this specific biomedical device most likely stems from design difficulties (multidisciplinary knowledge, coupling of measurements, sterility).

Simulated physiological fluids are extremely simplified (diluted saline solutions) deprived of bovine serum or organic species such as proteins [47]. However, the physiological environment is a key element in the degradation and biocompatibility of joint replacements. The fluid effectively conditions the physical integrity of metallic biomaterials by modifying the surface protective film (composition, structure and thickness), which largely governs its biocompatibility ability. More specifically, organic species adsorb and react with the surface of biomaterials, by complexing with metal ions, and may accelerate their ionic dissolution and, thus, the corrosion rate [48,49]. The surrounding environment, acting as a receptacle for degradation products, also affects the surface reactivity of wear debris [50] and the complexation of metal ions [49,51] which can affect cytotoxicity.

The physiological fluid is also of primary significance in cell culture as it provides all the essential elements for proliferation. As an example, some proteins can control the adhesion of cells to biomaterials [52]. In addition, the environment also contributes to cell viability by contributing a controlled supply of carbonate and oxygen, which maintains the pH and osmolarity within viable limits for the cells. Although most tribometers operate in a saline and aerated environment, confirming that they are not adapted to cellular conditions, some recent studies have proposed tribocorrosion devices, which can be inserted into an incubator [53] or enclosed in thermostatically controlled chambers. These proposed devices are promising examples to be followed for further evaluation of the biocompatibility of metallic biomaterials in direct contact with cells.

As previously mentioned, the degradation products of tribocorrosion (wear debris and ions) lead to an adverse cellular response involving osteoblasts, fibroblasts, and immune cells in the periprosthetic osteolysis mechanism. One of the most important cellular target for wear debris is the macrophage, which contributes to increased bone resorption. Micrometric-sized wear debris ($< 1\,\mu m$ in size) may be phagocyted by macrophages [54,55]. For example, polyethylene particles activate pro-inflammatory signalling, which leads to increased osteoblasts and osteoclasts recruitment and activation around the joint space (proteolytic enzymes, inflammatory mediators and osteolytic mediators) [6,7,19]. Although increasingly more studies are evaluating the effect of wear debris and metal ions on macrophages [56], bioassays generally involve monitoring cell viability, proliferation and mineralization over time and/or analysis of inflammatory cytokines in the supernatant [11,57]. The direct observation of living cells during testing could be used to complement post-testing biological analyses. However, this task is difficult because it requires powerful microscopy devices for acquisition, measurement regularity, and advanced image processing.

Herein, we presents a new biotribocorrosion set-up to simulate the physiological conditions of prosthetic joint contact, which was developed on the aforementioned limitations. The device was used for preliminary investigation of the tribocorrosion of a polyethylene/CoCrMo couple in a simulated macrophage environment. Two aggressive joint contact conditions were simulated to promote the production of polymer wear particles or metal ions. We focused on evaluating the degradation products and their effect on the cellular response of macrophages. The preliminary results allowed us to perceive the entire scope of the biotribocorrosion set-up as well as possible perspectives.

2. Biotribocorrosion Set-up

In this study, the bioreactor from a previous study [58] was specially adapted to achieve cellular physiological conditions that are representative of joint prosthetic contact. It was therefore possible to generate degradation products in the same environment in which the cells are grown. Adaptations to the bioreactor were made based on the specifications necessary for electrochemical, tribological and biological characterization.

2.1. Specifications of Biotribocorrosion Set-up

The development of the biotribocorrosion set-up was based on existing tribometers and their restrictions in terms of accurately representing a joint contact [20–24,59]. The specific criteria used in the development of the set-up included:

1. The use of cell culture conditions (cell culture medium, temperature, pH buffer, sterility), to enable the addition of living macrophages

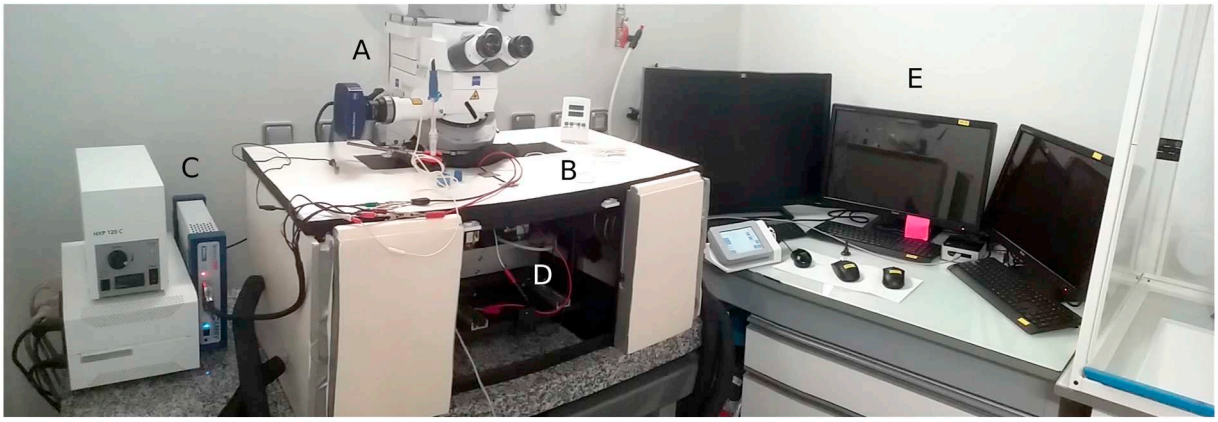

Fig. 1. Custom-built biotribocorrosion apparatus inside a clean room (ISO Cleanliness Class 5): A) fluorescence microscope, B) custom thermostatic enclosure, C) potentiostat, D) tribocorrosion apparatus and E) data acquisition computers.

near the simulated joint contact, which is more relevant during the early stages of the inflammatory reaction.
2. The use of fluorescence microscopy to enable evaluation of the proliferation of living cells (density, morphology) *in situ* and of the fluorescent polymer wear debris present in the environment or on friction surfaces after testing.
3. The elimination of intermediate steps (digestion and/or filtration) in the analysis of degradation products (wear debris and metal ions) that may affect their reactivity and cytotoxic nature.

These three points constitute the fundamental characteristics of the biotribocorrosion set-up. Therefore this device has the particularity of allowing *in situ* visualizing of the fluorescence of living cells, by enabling simultaneous measurement of corrosion and mechanical indicators during friction tests between two studied materials (Fig. 1, Fig. 2, Fig. 3). Although all friction couples were possible, we simulated the joint contact of an ankle prosthesis. According to large joint registry datasets, five year survival rates of ankle prostheses do not exceed 90% [60]. In addition, the failures of total ankle prostheses are typically secondary to loosening or instability resulting from the accumulation of metal ions and wear debris in the tissues [60]. It is therefore essential to study the wear particles produced from CoCrMo/polyethylene contact as well as metal ions to elucidate the adverse effects of ankle prostheses. The biotribocorrosion set-up developed in this study creates an environment that is conducive to the culture of macrophage cells while producing wear debris (essentially of polyethylene because of the hardness of both materials) and metal ions.

The device was based on a tribometer that was previously used for friction tests between an UHMW-PE tibial implant and a convex glass plate [58]. The modifications to this tribometer enabled the integration of an electrochemical setting (three-electrode set-up), a custom thermostatic enclosure including the mechanical device and a fluorescence microscope. The design and operation of the biotribocorrosion set-up are discussed in the following sections by disciplinary fields.

2.2. Electrochemical Measurements

A cobalt alloy (CoCrMo) disc was attached on the sample support (Fig. 2) containing the supplemented cell culture medium (RPMI-1640), which served as the physiological fluid (12 ml). For the electrochemical study, a conventional three-electrode set-up was used for corrosion assessment. The set-up consisted of a CoCrMo disc as the working electrode (WE), a platinum wire as the counter electrode (CE) and a saturated calomel electrode (SCE) as the reference electrode (E_{SCE} = +0.244 V/SHE). The surface of the counter electrode was larger than that of the working electrode (S_{CE}: 7.8 cm^2 > S_{WE}: 2.8 cm^2). The reference electrode was offset from the centre of the work cell using a Luggin capillary. This set-up was connected to a

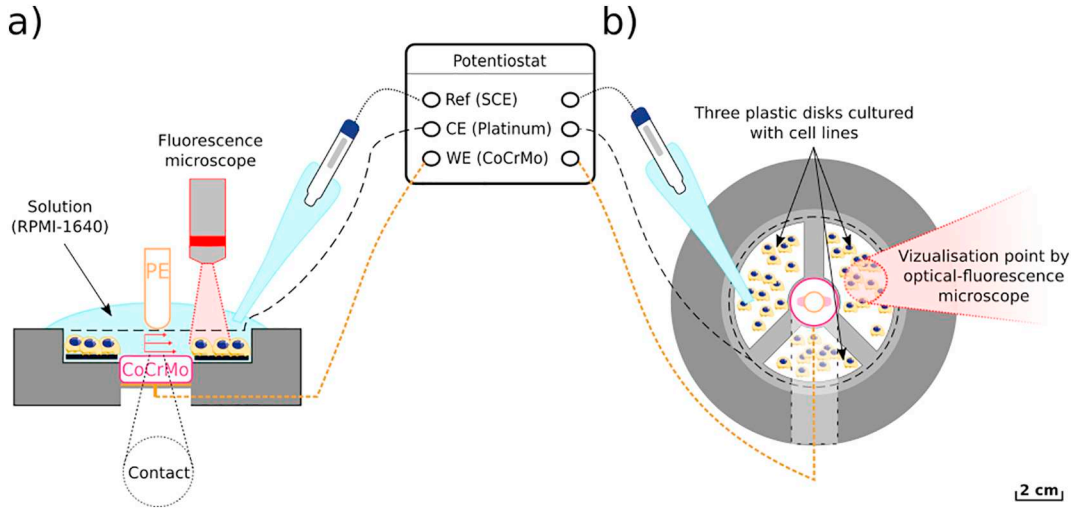

Fig. 2. Side view (a) and top view (b) of sample support, which included the following electrochemical set-up: a CoCrMo disc as the working electrode (WE), a platinum wire as the counter electrode (CE) and a saturated calomel electrode (SCE) as the reference electrode, and three discs machined from Petri dish with cell lines.

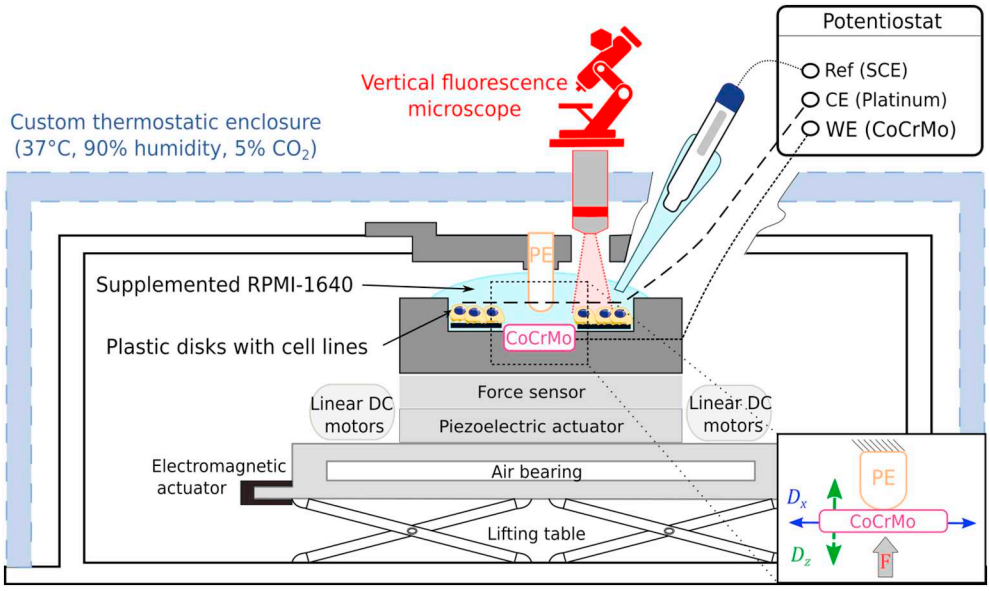

Fig. 3. Schematic view of experimental biotribocorrosion set-up adapted to cell conditions. The set-up consisted of a conventional three-electrode set-up, a pin-on-plate tribosystem and a vertical fluorescence microscope. The entire set-up was placed in a custom-made plastic enclosure, which was thermally and gas insulated. The mechanical contact was placed in the friction pin-on-plate system: an UHMW-PE pin against a CoCrMo disk. The contact pressure was fixed at 25 MPa by adjusting the lifting table in the vertical direction (D_z). The sliding displacement was controlled to be between 0.6 and 2 mm/s in the horizontal direction (D_h) by the linear DC motors.

potentiostat Gamry Inst. Reference 1000, which was controlled using Gamry Framework 6.32 software. The electrochemical installation enabled the measurement of the open circuit potential (E_{OCP}) as well as the polarization the CoCrMo by applying potential or intensity. For the experimental conditions in this study, only the E_{OCP} was recorded, which provided information on the dissolution and repassivation of the passive film of CoCrMo under mechanical stimulation.

2.3. Tribosystem

To represent the stresses on ankle prostheses, a reciprocating pin-on-plate bench wear test was used, based on an alternative movement [61]. This set-up makes it possible to consider various numbers of cycles and latency times to simulate load cycles such as those in walking. The tribometer has a fixed frame that holds the pin support while the metallic sample is mobile (Fig. 3). The translation movements and load were applied by the lower part of the system using a lifting table (NORELEM, France). The force was controlled by a feedback loop to keep it constant during testing. The force was fixed at 35 N with a bending radius of 48 mm, which produced an initial contact pressure of 25 MPa using the Hertz model. The load value was fixed according to the real average compressive load per unit area which varies between 3 and 5.2 times the body weight [62,63] and corresponds to the contact pressure of ankle replacements (between 5.7 and 25 MPa) [64–66]. The load was measured by a three-axis force sensor (K3D60 ± 100 N, Testwell, France), and the shear force was measured by a piezoelectric sensor (PZ 100 SG, TRIOPTICS, France). The friction coefficient (COF) is defined as the ratio between the shear force (once the surfaces slide against each other) and the normal load. The horizontal translation displacement of the sample holder was driven by a linear DC motor (H2W Technologies, USA). The friction distance was set to 10 mm with a reciprocating frequency of 50 or 200 mHz (0.6 or 2 mm/s respectively). The friction test time was set between 3 h30 and 5 h30 because the aim was to reproduce the maximum use time of an ankle prosthesis can undergo in a working day. The total duration was between 5 and 7 h. The entire tribometer was controlled by using a modified version of the Galil software (A2V Mecatronique, France), renamed Biolub, allowing the visualization the normal force F_z, tangential force F_y, vertical displacement D_z and horizontal displacement D_h in real time. Determination of the total wear volume was possible at the end of the test using optical profilometry measurements.

2.4. Custom Thermostatic Enclosure

To achieve a proper temperature and concentration of dissolved gas (oxygen and carbon dioxide) representative of those in the body environment, the biotribocorrosion tests were performed in a custom-made thermostatic enclosure. The enclosure was made from plastic plate covered with insulation and was constructed to satisfy the following conditions: **i)** surround the tribocorrosion set-up, **ii)** allow the visualization of the cells by fluorescence microscope at any time, **iii)** be heat and gas insulated, **iv)** maintain stable conditions: temperature (37 °C), humidity (90%) and air content (5% CO_2), **v)** be easily modified. This chamber corresponds to a non-automated incubator. The temperature was kept constant at 37 °C by circulating water from a heating circulator (Polystat 37, Fisherbrand, Fisher Scientific) through plastic and copper wires. The temperature was monitored using a digital thermometer. The CO_2 content was injected from a sterilized CO_2 gas bottle (N48, Air Liquide, France) and controlled by a wireless sensor (PASCO, PS-3208) driven by PASCO Capstone software. The humidity was maintained using two beakers filled with distilled water.

2.5. In Situ Observation of Living Macrophages by Optical Fluorescence Microscopy

The tribological and electrochemical analyses were completed by *in situ* visualization of a mouse macrophage cell line (RAW 264.7) around the contact using an optical light and vertical fluorescence microscope (Zeiss Axio Examiner Z1, Leica DMLM). The microscope was equipped with a CCD camera (Leica DC350F) with two objectives: a "Fluar" 5 × / 0.25 M27 (focal distance = 12.5 mm) and N-Achroplan 63 × /0.9 M27 (focal distance = 2.4 mm) and two laser lines (488 and 555 nm) coupled to a fluorescence camera (Axio Camera 60 N-C). The cell viability and morphology were assessed using two markers: **i)** a lipophilic membrane marker (dialkyl aminostyryl dye: Dil, Thermofisher) labelled in orange-red (λ_{ex} = 549 nm and λ_{em} = 565 nm) and **ii)** an intracellular pH marker (pHrodo™ Red AM, Thermofisher) labelled in red (λ_{ex} = 560 nm and λ_{em} = 585 nm). The membrane and intracellular pH labelling did not appreciably affect cell viability, development, or basic physiological properties. The cells were washed with phosphate-buffered saline solution (PBS) post treatment, incubated with 5 µl diluted in 6 ml of supplemented RPMI-1640 or with 60 µl (pHrodo™) for 30 min, and washed with PBS before imaging. Fluorescence microscopy imaging was performed *in situ* during the tribocorrosion tests. The morphological characteristics of the cells were quantified using ImageJ

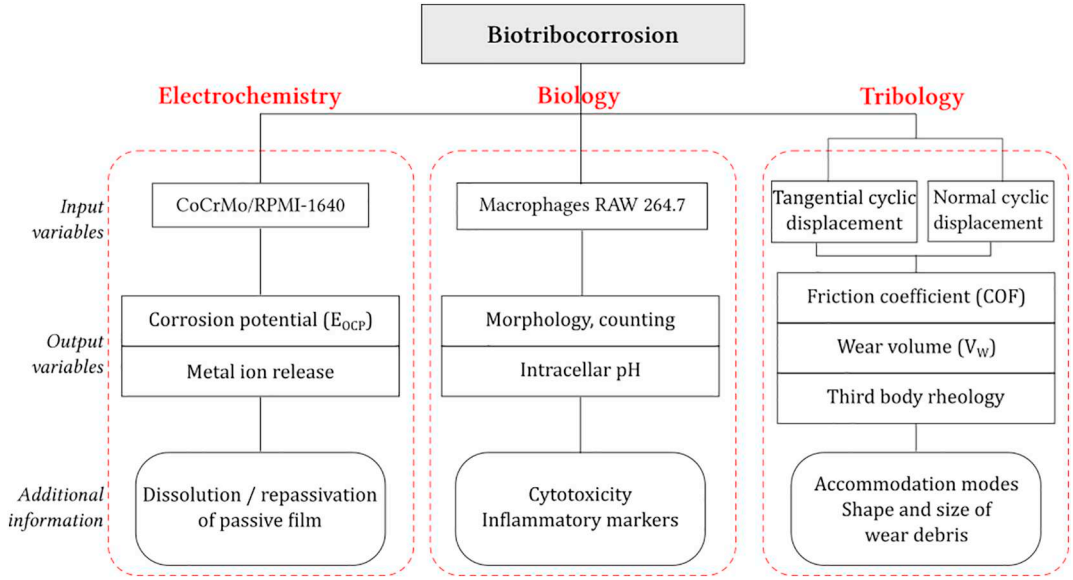

Fig. 4. Synthetic diagram of biotribocorrosion experiments with inputs and outputs variables complemented by characterization techniques.

software (NIH, USA) through binarization treatment, particle area analysis and distribution calculation.

2.6. ISO Cleanliness Class 5

The biotribocorrosion tests were performed in a clean room (ISO Cleanliness Class 5) located in LaMCoS (CNRS, INSA Lyon, UMR 5259). The environment maintained a level of cleanliness equivalent to ISO Cleanliness Class 5, i.e. < 100,000 particles with size of 0.1 µm or larger per cubic metre, or < 832 particles with size of 1 µm or larger per cubic metre. The main parameters that control the environmental performance of a cleanroom are the air flows and pressure difference. By adjusting the air flows, a positive differential pressure can be created to prevent the introduction of potential contaminants from the surrounding clean room. The temperature, humidity, and cleanliness were also controlled.

2.7. Synthesis of Experimental Inputs and Outputs

The experimental parameters and data obtained from the biotribocorrosion set-up are summarized in Fig. 4. The device allows variation of the input data from three scientific domains and the deduction of additional information on biotribocorrosion. Many post-test analyses are possible, however, only those that were performed as part of this study are marked. Details of these analyses will be discussed in Section 3.5.

3. Materials & Methods

3.1. Sample Preparation

Metallic plates were made from medical grade cobalt chrome molybdenum (CoCrMo) alloy (Biodur® CCM® from Carpenter) following ASTM-F1537–11 and ISO 5832-12:2007. The surfaces were mirror polished (Marle Company, France) to roughness R_a < 0.04 µm. Before testing, the samples were ultrasonically cleaned in a bath of ethanol for 10 mins, wiped, exposed to UV light for 30 mins for sterilization and then placed for 24 h in a humidified atmosphere consisting of 95% air and 5% CO_2 at 37 °C. This final preparation step resulted in a reproducible surface state with a controlled chemistry. A homogeneous and stable native oxide is then formed on the surface. This surface preparation limit the dispersion of the results. Indeed, passive film grown directly in the solution is sensitive to the last preparation step (polishing, storage atmosphere and duration, …). The CoCrMo discs were then inserted into the sample holder surrounded by a sealing ring with copper adhesive tape at the base to ensure good electrical contact (Fig. 2).

An ultra-high-molecular-weight polyethylene (UHMW-PE) pin formed the contact with the lower surface of the metallic plate. Because the same polymer (Chirulen® 1050, Quadrant MediTECH, USA) is used for all joint prostheses (hip, ankle and knee), UHMW-PE pins were drilled from the insert between the cup and femoral stem of standard double mobility prosthesis inserts (HDM248, TORNIER) to obtain pins of large volumes. The UHMW-PE polymer conformed to ASTM F648, ISO 5834-1, and ISO 5834-2. The polymeric pins were cleaned with soap and deionized water, and their surface condition was examined using optical profilometry (0.2 rms roughness) before testing.

3.2. Test Fluid

The solution consisted of a classical cell culture medium composed of Roswell Park Memorial Institute (RPMI-1640; Dominique Dutscher, France) medium supplemented with 10% foetal bovine serum (FBS; Dominique Dutscher, France) and 1% antibiotic-antimycotic (Pan Biotech 100 U/ml of penicillin, and 100 mg/ml of streptomycin). The pH varied from approximately 7.4 to 7.6 and was stabilized by a controlled CO_2 content (50,000 ppm) via the carbonate buffer. The mass formulation of inorganic ions and the main organic compounds of RPMI-1640 are given in Table 1. The inorganic salt concentrations were generally close to those of synovial fluid [67]. Chloride ions, known for their tendency to initiate passive film degradation and dissolution of metallic materials, are not overestimated in RPMI-1640; soluble organic molecules such as proteins, vitamins, and glucose act as nutrients for cells, but can also adsorb to solid surfaces by forming soluble complexes with metallic ions. The adsorption of these biomolecules is therefore a decisive factor in the dissolution of metal alloys.

3.3. Cell Culture

Macrophages were selected for culture because they are the main cells associated with particulate phagocytosis in the inflammatory reaction at the bone implant interface. The murine macrophages cell line RAW 264.7 (ATCC® TIB-71™) was used because of its well-defined biological function and availability. The cell lines were cultivated in

Table 1
Ionic molar and organic concentrations of RPMI-1640 (mM).

Ionic salts								
Na^+	Cl^-	HCO_3^-	HPO_4^{2-}	K^+	NO_3^{2-}	Ca^{2+}	Mg^{2+}	SO_4^{2-}
129.29	108.03	23.81	5.64	5.37	0.42	0.42	0.41	0.41
Organic compounds								
Amino acid			Vitamin			Other		
L-Arginine		1.15	B3		0.41	D-Glucose		11.1
L-Leucine		0.38	Myo-inositol		0.19	Phenol red sodium salt		0.01
L-Isoleucine		0.38	Choline chloride		0.02			
L-Asparagine		0.33						
L-Serine		0.29						
L-Lysine		0.22						
L-Cysteine		0.21	*Other amino acids and vitamins are present at lower concentration.*					

supplemented RPMI-1640, changed three times per week and kept in a humidified atmosphere of 95% air and 5% CO_2 at 37°C. For the biotribocorrosion tests, the cells were cultured on three discs machined from the bottom of a 10 mm diameter Petri dish (Sigma-Aldrich, France) (Fig. 2). To assess the cytotoxicity of CoCrMo, the macrophages were cultured on metal discs that has been previously UV sterilized for 40 min. The seeding density of the cell lines, controlled by a cell counter (Millipore™ Scepter, Dutscher), was between 3 and 5×10^4 cells/cm^2 for macrophages with 2 days for proliferation before testing.

3.3.1. Viability Test using MTT[1] Assay

MTT viability tests were performed at 24, 48 and 72 h to measure the effect of CoCrMo on the macrophages. In summary, MTT is transformed by living and metabolically active cells into purple formazan crystals, which can be measured after solubilization in dimethyl sulfoxide (DMSO) at 570 nm. The cells were incubated at 37 °C for 4 h with 0.125 mg/mL MTT (final concentration) according to the previous work procedure [68]. Then, medium containing MTT was removed, and the formazan crystals were solubilized with 4 ml of DMSO per well. The absorbance of the cells cultured on the CoCrMo discs indicated the cell viability on the surface of the biomaterial. The values were compared with those of the control without a biomaterial sample (assuming 100% viability).

3.3.2. Cytotoxicity Test by Lactate Dehydrogenase (LDH) Assay

The cytotoxicity tests were performed at the same time as the viability tests at 24, 48 and 72 h. Lactacte dehydrogenase is a cytosolic enzyme that is released into the culture medium for cell damage. Extracellular lactacte dehydrogenase LDH was detected in 200 µl culture media using an LDH cytotoxicity assay kit (Pierce; ThermoFisher Scientific), as specified by the manufacturer. A sample without the CoCrMo biomaterial was used as a negative control and, reference for 0% cytotoxicity. In addition, a positive control (10% Triton X-100 (*v/v*)) was added to the cells to induce complete LDH release and was used as a reference for 100% cytotoxicity. The results are represented as a percentage of cytotoxicity compared with the control without the biomaterial.

3.4. Testing Protocol

3.4.1. Typical Steps for Biotribocorrosion Test

Biotribocorrosion tests require fine sample preparation (CoCrMo, UHMW-PE and cells) as well as a structured sequence of experimental tasks. During this project, a protocol using mechanical, electrochemical and biological parameters was established to optimize the quality of the data obtained. The entire process was coordinated in different stages (Fig. 5):

The initial stationarity (Init) of 30 min enables verification that the OCP corrosion potential, temperature, and CO_2 rate are constant. It is performed without mechanical contact. Fluorescence imaging enables information of the morphology of the cells at the beginning of the test.

Then, the tribocorrosion test was divided into three steps: compression stress relaxation, rheology and friction (Fig. 5):

1. Compression stress relaxation (CSR) consists of applying a normal load (35 N) on the CoCrMo against the UHMW-PE pin. The force is maintained for 15 min to accommodate the relaxation effects of the machine. This step also provides information on the viscoelasticity of the third body on the Tribological Transformation of Surface (TTS) of UHMW-PE.
2. The second phase, rheology testing (Rh), consists of completely (Fig. 5b-2') or partially (Fig. 5b-2") discharging the contact. The load is then maintained at 5 N for 5 min and vertical sinusoidal movements (D_z) of 40 µm amplitude are performed at frequencies of 0.5–2 Hz. This step promotes the ejection of UHMW-PE wear debris out of contact. It is possible to characterize the third-body rheology by determining its elastic force F_e, viscous force F_v and modulus of elasticity E. The rheology step also leads to convection movements, which can promote metal ions dissipation in solution and therefore expose them to cells.
3. During the sliding testing (Slid.), the vertical displacements are then replaced by horizontal displacements (D_x) of 10 mm amplitude with sliding displacement of 0.6 or 2 mm/s. The load is again charged at 35 N. The friction between the UHMW-PE and CoCrMo lasts for 1 h30.

The tribocorrosion cycle, consisting of phases CSR, Rh and Slid is repeated three times. The values of the corrosion potential (OCP), normal and tangential forces and horizontal displacement are recorded. Fluorescence imaging was performed after each sliding sequences during the CSR + Rh sequences.

Final stabilization (Final) closes the biotribocorrosion assay by removing normal contact loading and controlling the cell morphology by fluorescence. The entire biotribocorrosion test procedure takes 8 h.

3.4.2. Experimental Conditions used in the Present Paper

Two experimental conditions were used set to promote the formation of either polyethylene wear particles (Test No. 1) or metal ions (Test No. 2) because these products correspond to the main degradation products leading to biological inflammation and complications in the joint contact. The main experimental parameters are summarized in Table 2. The differences between both biotribocorrosion tests are of mechanical (surface condition of CoCrMo, sliding velocity, loading during rheology sequence) and biological (fluorescent marker, cell density).

[1] 33-(4,5-dimethylthiazol-2-yl-)2,5-diphenyltetrazolium bromide

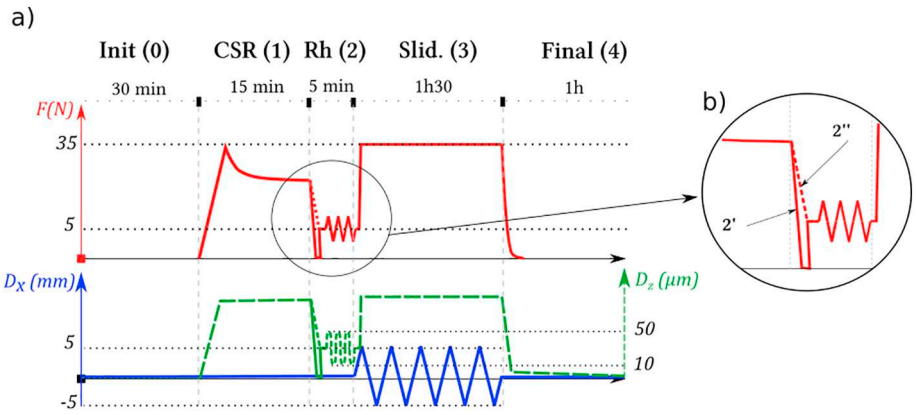

Fig. 5. a) Schematic illustration of protocol for biotribocorrosion tests including the following major phases: initial stabilization (Init), compression stress relaxation (CSR), rheology sequence (Rh), sliding (Slid) and final stabilization (Final). D_z and D_x correspond to the vertical and horizontal displacements, respectively. b) Variants of the rheological sequence with complete (2′) or partial (2″) discharge of the load (F).

Table 2
Main experimental parameters of biotribocorrosion tests (No. 1 and No. 2).

Nature of experimental parameters		Test No. 1	Test No. 2
Materials and solution	Metal alloy	CoCrMo (ASTM-F75) disc	
	- Finishing surface	*SiC* 1200	Mirror polishing
	Counterpart	UHMW-PE pin	
	Test fluid	Supplemented RPMI-1640	
Biological	Cell lines	RAW 264.7 (macrophages)	
	- Density [$\times 10^4$ cells/cm^2]	5	3
	Fluorescent marker	Lipophilic membrane	Intracellular pH
Mechanical	Calc. Hertzian average pressure [MPa]	25	
	Amplitude of displacement [mm]	10	
	$V_{Sliding}$ [mm/s]	0.6	2
	Loading during rheology sequence (Rh)	Completely discharged (Fig. 3b-2')	Partially discharged (Fig. 3b-2")
	Duration [h]	5–7	

3.5. Post-Testing Characterizations

Additional information on biotribocorrosion processes can be obtained by post-test characterization and analysis, which provide the composition of the passive film, the amount of metal ions and their effect on the cell viability, and the analysis of the polyethylene wear debris.

3.5.1. UHMW-PE Wear Rate

Profiles of the surface lines and wear measurements of the UHMW-PE pins were obtained before and after the biotribocorrosion tests using a non-contact optical profilometer (Altisurf© 500, Altimet). The acquisition speed was set at 40 mm/s with a non-contact resolution of 12 nm. The samples were placed on a rotating base allowing a profile measurement every 10° along a reference line. This method enables the entire surface of the pin to be swept and establishes a contact zone after rubbing. The MountainsMap software automatically performs standard calculations such as estimating the radius of curvature of the measured profile, extracting the profile area and signal processing (levelling, reflectivity variations). The profile lines of three angles on the wear track were used to estimate the polyethylene wear volume.

3.5.2. Wear Debris Analysis

Environmental scanning electron microscopy (ESEM, FEI Company, Quanta™ 600, Tungsten W) was used to analyse the UHMW-PE pin surface. An electron gas detector was used to capture topological information from the surface. The images obtained with the secondary electron detector were taken using an acceleration voltage of 5–10 kV, a working distance of 10–13 mm and a diaphragm aperture of 60 μm.

Polyethylene wear debris fluoresce under a 555 nm laser, whereas CoCrMo alloy is not fluorescent. For this reason, polymer debris and adhesive layer were observed both on the metallic surface and in the extracted cell culture medium. A sample of the supernatant was gelled in an agar-agar solution, which preserved the shape of the polymer wear debris. Fluorescence images of representative areas of the wear track were obtained using the vertical fluorescence microscope mentioned previously. The number of particles and, area (A) and perimeter (P) of each particle were measured using Image J software (NIH, USA). A minimum of 10 fluorescence images at a magnification of 63× (N-Achroplan 63×/0.9 M27, Zeiss) were evaluated, yielding between 5,522 and 15,149 particles. The equivalent circle diameter (ECD) and equivalent shape ratio (ESR) were computed to determine the particle size and morphology, respectively, based on the guidelines for particle analysis outlined in ASTM F1877-16 [69]. UHMW-PE wear debris particles from the lubricant, trapped in an agar-agar solution, were examined under the fluorescence microscope at a lower magnification of 5× (Fluar 5×/0.25 M27).

3.5.3. Inductively Coupled Plasma Mass Spectrometry (ICP-MS)

Supernatants of RPMI-1640 were collected before and after the tests and examined using inductively coupled plasma mass spectrometry (ICP-MS) to quantify the released metal ions. The solutions were analysed using an iCAPTM TQs ICP-MS (Thermofisher Scientific, Bremen) with Triple Quadrupole Technology. The Cr, Co and Mo elements of molar masses 52, 59 and 95 g.mol^{-1} respectively were quantified with a detection limit of 0.05 μg/l. The ICP-MS analyses were performed by the Geochemistry Laboratory, ENS Lyon, France (Philippe Telouk).

3.5.4. Inflammatory Cytokines Measurement

The concentration of cytokines in the supernatants obtained from cell cultures were quantified using the sandwich immunoassay (ELISA) method. The amount of prostaglandin E_2 (PGE_2) produced by the macrophages and released into the media was quantified using a commercially available competitive binding radioimmunoassay kit, in accordance with the methodology recommended by the manufacturer (Cayman Chemical, Ann Arbor, MI). The absorbance was obtained

using reader plates at 405 nm. The concentrations of cytokines (pg/ml) were calculated from a standard curve of recombinant cytokines and normalized by the total amount of proteins released by the cells into the extracellular medium.

3.6. Statistical Methods

The error bar of the metal ion rate corresponds to the detection limit of the ICP-MS device. The distribution of the particle shape and size (ESR and ECD factors) and cell distribution were automatically analysed by ImageJ software. The statistical differences between tests were calculated using a single-factor analysis of variance, with $p < .05$ as the significance level. Although some distributions of particle size and mean cell surface area were not precisely Gaussian, the large sample size justified the use of this parametric analysis. The error bars of the wear rate and the number of UHMW-PE particles in the medium correspond to the standard deviation of at least five independent measurements.

4. Results

4.1. Electrochemical Measurements

The open circuit potential (OCP) measurements are presented in Fig. 6. These experiments were performed on three CoCrMo samples (Control, Test No. 1 and No. 2) immersed in supplemented RPMI-1640. The environmental conditions were identical for all the tests (37 °C, 5% CO_2). The control sample was not subjected to mechanical solicitations. The other samples (named test No. 1 and No. 2) were subjected to wear.

In supplemented RPMI-1640, without sliding, the potential of CoCrMo increased from −160 to −50 mV/SCE. A preliminary study characterized these potential values as being included in the passivation field of the CoCrMo. Even if the potential did not reach the steady state, the passive film can be considered as grown during this measurement.

Under tribological testing, the variations in the OCP were measured according to the biotribocorrosion testing protocol. Each measurement was characterized by several transient phenomena. Fig. 7 and Fig. 8 detailed the evolution of the OCP for Test No. 1 and 2, respectively.

During Test No. 1, the OCP potential gradually increased over time from −260 to −150 mV/SCE (Fig. 7a). This evolution follows that recorded for the control sample. Before the first sliding sequence, the potential was closed to -250 mV/SCE, which is consistent with the corrosion potential of CoCrMo in supplemented RPMI-1640 in an incubator. When the force was loaded (0.3 h) and sliding started, a small

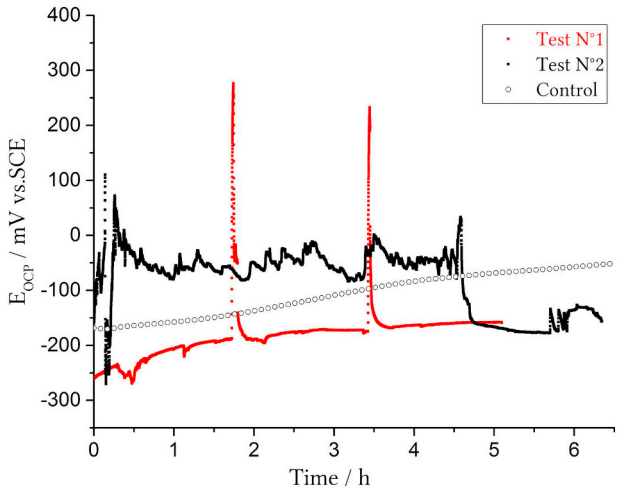

Fig. 6. OCP variations during biotribocorrosion tests for CoCrMo samples immersed in supplemented RPMI-1640. The control sample was not subjected to mechanical solicitation.

negative drop in potential (30 mV) was observed, corresponding to the action of mechanical stress on the growth of the passive film on CoCrMo. The potential curve tended to reach the initial evolution by gradually increasing. Fig. 7b shows the electrochemical potential noise measured during sliding for Test No. 1. The signal disturbance cannot be related to the movement of the pin on the metal surface. During the compression stress relaxation and rheology (Fig. 7), the potential suddenly increased in the range of 200–300 mV/SCE. This experimental sequence mechanically consisted of the release of the load and vertical movements of 40 µm amplitude. This step was performed twice, and the potential followed the same evolution, as if this sequence did not disturb measurements. At the end of the sliding (sequence 3), no significant evolution of OCP was observed. During this measurement, the OCP was located in the passive state of the CoCrMo.

The potential response recorded for Test No. 2 differed from that obtained for the previous sample. At this step of the analysis, the different surface preparation for the two tests should be considered. The initial potential is higher than that in Test No. 1, increasing from −150 to 0 mV/SCE (Fig. 8a). The OCP curve is noisy, with a sharp transient at the loading of the force (0.35 h) (Fig. 8b). The potential is characterized by many current transients around a median value of 5 mV/SCE. Several noise scales can be considered: the first concerns the current background noise already recorded for Test No. 1, highlighted in Fig. 8c; the second one exhibits rapid variations on a wide scale of potential.

In the latter case, the OCP disturbances may be related to the sliding interactions between the pin and the passive film grown on the metallic surface. The signal repetition pattern every 5 s corresponds to the time required for the pin displacement. Unlike for Test No. 1, the potential did not increase during the compression stress relaxation and rheology sequences. In this case, the sequence mechanically consisted of the release of the load at 5 N and vertical movements of 40 µm amplitude.

4.2. Metal Ion Release

At the end of the experiments, the supernatants were analysed using ICP-MS to quantify the amount of released ions from wear and dissolution of CoCrMo. Fig. 9 shows the Co, Cr, and Mo contents in the solution after the biotribocorrosion tests and the immersion test of CoCrMo in supplemented RPMI-1640 for 6 h in an incubator (Control). Cobalt was the most highly concentrated of the three detectable elements, followed by chromium and molybdenum. This result was expected because of the chemical composition of the alloy, which contains up to 64.4 wt% Co. The total release of cobalt ions was stabilized or reduced in the tribocorrosion tests compared with in the immersion test (from 116 to 70.7 ppb). However, the levels of Mo and Cr ions increased for the biotribocorrosion tests because of the surface preparation of the sample. This result was expected because the friction of the pin on the CoCrMo leads to the disturbance of the passive film. The release of Cr alone was approximately 1.5–2.5 times higher under the biotribocorrosion conditions (12 and 22.9 ppb for Test No. 1 and 2, respectively) compared with the control (8.8 ppb). Similarly, the molybdenum ion content was higher for the conditions of Test No. 2 (8 ppb) than for those of Test No. 1 (6 ppb), which is close to the control level (5.7 ppb).

4.3. Wear Mechanisms

The friction coefficient (COF) during a cycle was not stable (results not shown). For Test No. 1, adherence peaks were observed in the friction curve. The static friction force, which is necessary to initiate sliding, was higher than the dynamic force required for continuing the motion in the steady state. This sequence of static-to-dynamic friction was measured after every reversal of the sliding direction. Adherence peaks were also observed for the Test No. 2, but only for one sliding direction.

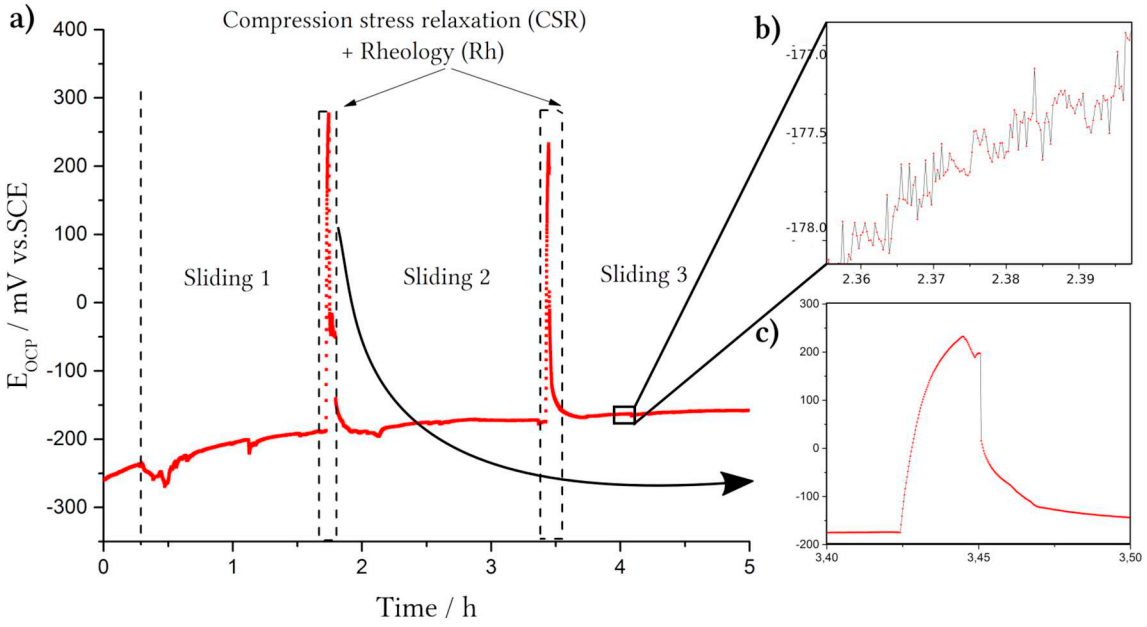

Fig. 7. Evolution of the open-circuit potential before and during intermittent sliding tests performed at 35 N and 0.6 mm/s on CoCrMo immersed in supplemented RPMI-1640 (Test No. 1) with focuses on b) electrochemical noise signal and c) during rheology sequence.

Fig. 10 presents the average calculated friction coefficient for each of three sliding sequences. The friction coefficient was higher for Test No. 1 than for Test No. 2 throughout the duration of the bio-tribocorrosion experiments. The friction value changed with time: it decreased slightly for CoCrMo No. 1 (from 0.1277 to 0.086), whereas a sharp decrease was recorded for CoCrMo No. 2 (0.1356 to 0.032 at the last sliding). The COF values were low, indicating that more than the half of the energy of the normal force exerted goes into retarding the lateral motion between the two surfaces *i.e.* low friction.

4.4. Wear Rate of UHMW-PE

The mean wear rate of the UHMW-PE pins was determined using optical profilometry measurements from the difference in the surface profiles before and after testing. The volume loss was calculated from surface area measurements obtained at three different angles. The wear rate for UHMW-PE for Test No. 1 and No. 2 was 0.167 ± 0.038 mm^3 after 5 h and 0.017 ± 0.010 mm^3 after 7 h respectively, corresponding to 11.173 ± 2.569 mm^3/MC and 0.945 ± 0.557 mm^3/MC, respectively (results not shown). The volume loss was five times lower for Test No. 2 than for Test No. 1, suggesting that the surface conditions affect the wear rate.

4.5. Surface Analysis

The size, shape, nature and number of polyethylene wear particles were analysed by examining the UHMW-PE and CoCrMo surfaces. SEM photomicrographs of the wear scars on the UHMW-PE pins are

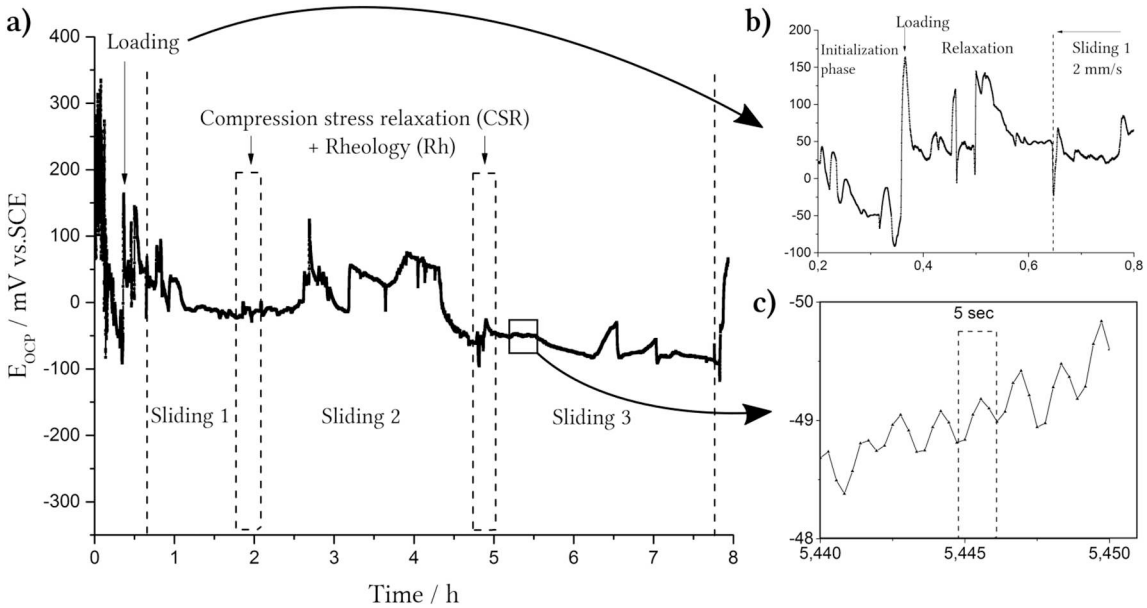

Fig. 8. Evolution of the open-circuit potential before and during intermittent sliding tests performed at 35 N and 2 mm/s on CoCrMo immersed in supplemented RPMI-1640 (Test No. 2) with focuses on b) charge loading part and c) electrochemical noise signal.

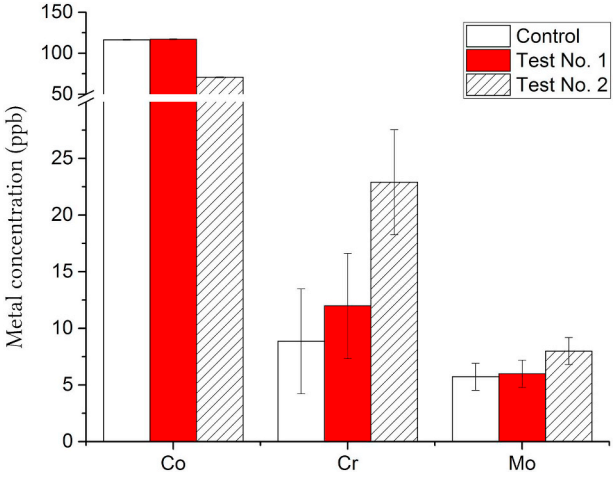

Fig. 9. Release of metal ions after biotribocorrosion experiments compared with immersion test of CoCrMo in supplemented RPMI-1640 for 6 h (Control). The error bars correspond to the detection limit of the device, which was 0.5; 4.6 and 1.2 ppb for Co, Cr and Mo, respectively.

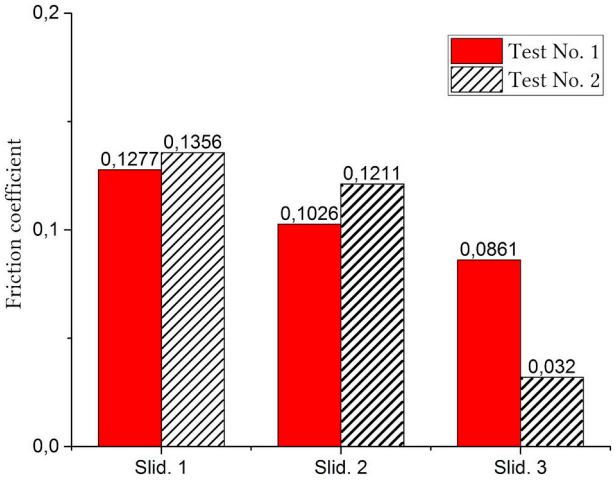

Fig. 10. Average coefficient of friction for UHMW-PE against CoCrMo in supplemented RPMI-1640 after sliding 1, 2 and 3 of the biotribocorrosion experiments.

presented in Fig. 11. The contact areas, delimited by dotted circles, were characterized by grooves perpendicular to the machining lines for Test No. 2 and oriented at 45° for Test No. 1. The polymeric particles were round, oval, or roll-shaped (as indicated by the arrows in Fig. 11). They are mostly round for Test No. 1, whereas they were crushed roll-shaped particles in the contact area for Test No. 2. An adherent and pulled UHMW-PE layer was also observed for the second case.

Fluorescence microscope images of the CoCrMo wear tracks produced in the biotribocorrosion tests are presented in Fig. 12. Fluorescence of the polyethylene wear particle was observed, coloured in red. The distribution and number of UHMW-PE particles varied significantly in the wear track. For Test No. 1, many small round particles were present whereas much fewer and more elongated particles were observed for Test No. 2. In addition to the wear trace, for both tests, the wear debris were larger and present up to the cobalt disc periphery. As observed in the SEM images of the pin, roll-shaped particles were present after Test No. 2.

Image analysis of the fluorescence micrographs was performed using a threshold in ImageJ software (NIH, USA). The individual particle area and perimeter were determined. The resulting area and dimensions (Fig. 13) were used to characterize the particle concentration, size (equivalent circular diameter ECD), and shape (aspect ratio ESR).

The ESR factor provides information on the shape of the particles: between 0 and 1.5, the particles are round, between 1.5 and 3, they are elongated, and beyond 3, they are fibrillar. For both tests, the majority of particles were in the ESR ranges of 1.5–3 (30%–37%) and 4.5–6 (35%–44%) (Fig. 13 a). Morphological quantification of the polyethylene particles on the surface of CoCrMo revealed that they were more elongated for Test No. 1 (37%) and more fibrillar for Test No. 2 (44%). Taking into account all the detected particles, the difference in shape for the two tests was not significant. The average ESR was approximately 4, indicating fibrillar-shaped particles (Fig. 13 c).

The ECD factor is used to qualify particles according to their size. The distribution of polyethylene particles was similar for both tests, and the frequency decreased with increasing size. The smallest particles (between 0 and 5 µm in size) were, in the majority, representing 69% of the particles for Test No. 2 and 49% for Test No. 1 (Fig. 13 b). Above 5 µm, the number of particles decreased with increasing size. UHMW-PE particles with an ECD > 5 µm were always more numerous in Test No. 1 than in Test No. 2. The size distribution differed significantly between the two tests: the polyethylene wear debris was 3 times less numerous (5,549) and 2.3 times smaller (ECD: 6 µm) for Test No. 2 than for Test No. 1 (15,149 particles with an average diameter of 14 µm) (Fig. 13 c).

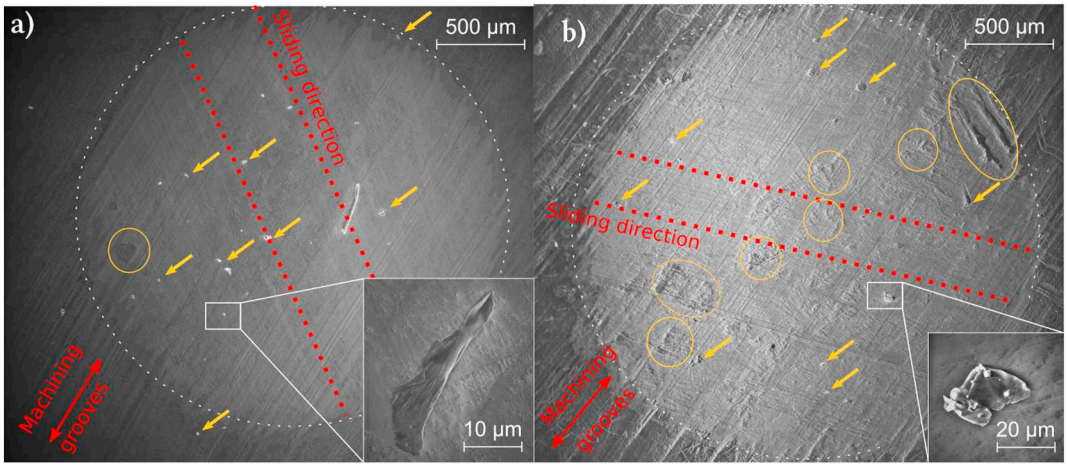

Fig. 11. SEM photomicrographs showing the UHMW-PE pins surface after biotribocorrosion Test No. 1 (a) and No. 2 (b). The arrows indicate wear particles and the circles indicate the thick third-body.

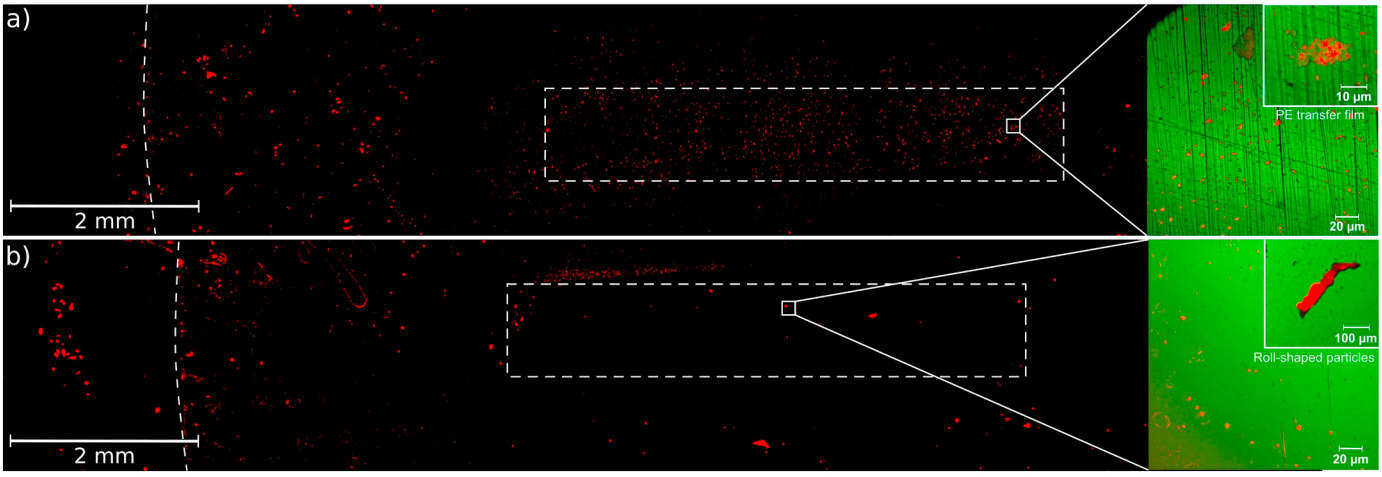

Fig. 12. Fluorescence microscope images of CoCrMo surface (black or green) with polyethylene wear debris (red) for biotribocorrosion tests: a) No. 1 and b) No. 2. The dotted areas represent the wear tracks. (For interpretation of the references to colour in this figure legend, the reader is referred to the web version of this article).

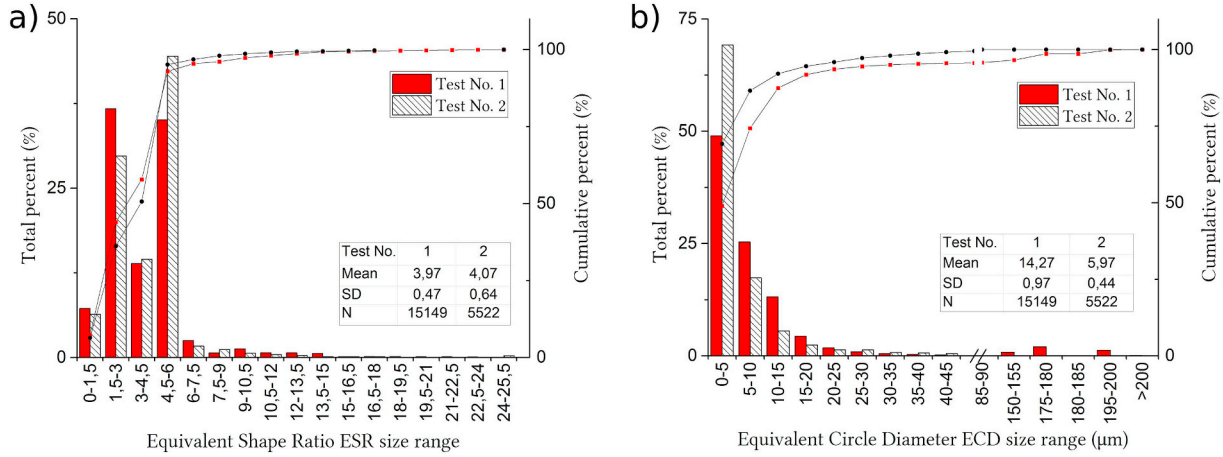

Fig. 13. Large distribution of polyethylene wear particles observed on the CoCrMo surface by a) shape (ESR) and size (ECD) parameters completed by c) mean and standard deviation of both ratios.

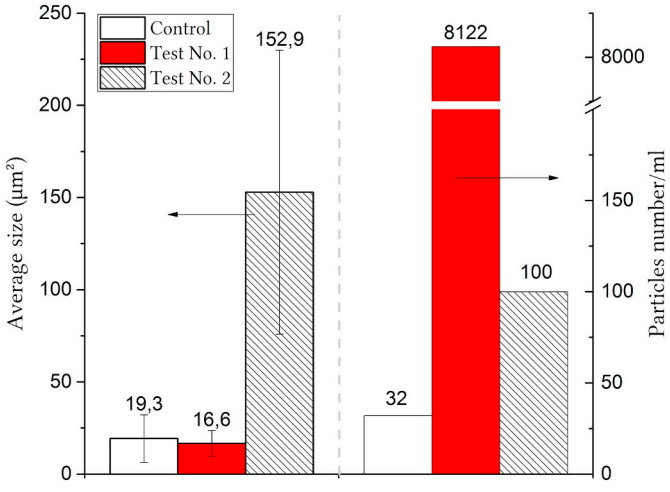

Fig. 14. Frequency and average size of polyethylene wear particles extracted from the supplemented RPMI-1640 after testing. The control values refer to supplemented RPMI-1640.

To complete the morphological analysis of the polyethylene wear debris, the gelled supernatant was also analysed using fluorescence microscopy. The sampling of the RPMI-1640 solution gelled with agar-agar, enabled to obtain complete quantitative information for the particles. The results of the analysis are presented in Fig. 14. The number of generated particles was clearly higher for Test No. 1 (8,122 particles/ml) than for Test No. 2 (100 particles/ml). In both cases, the concentrations were higher than that those obtained for a sample of RPMI-1640 solution, which served as a control (32 particles/ml). This low concentration most likely corresponds to polluting fluorescent particles that were trapped during gelling of the supernatant. The calculated average surface area of the particles generated after Test No. 1 was similar to that of the control (16.6 and 19.3 µm^2), whereas it was almost 10 times higher for Test No. 2 (152.9 µm^2).

4.6. Biological Analysis

MTT staining assays and LDH assays were performed on a mouse macrophage cell line (RAW 264.7) grown on CoCrMo. Measurements were taken at 24, 48 and 72 h after seeding the cells on CoCrMo disks. These analyses were used to verify the viability/proliferation of macrophages (MTT test) and possible CoCrMo-induced cytotoxicity (LDH test). The absorbance values were converted into percentages and are presented in Fig. 15. The results were not significantly different ($p > 0.05$), after 72 h with or without CoCrMo material, indicating that it does not induce cytotoxicity on RAW 264.7 cells. The negative percentages are because the measured absorbance was lower than those of the control sample. Thus, the CoCrMo alloy did not significantly affect

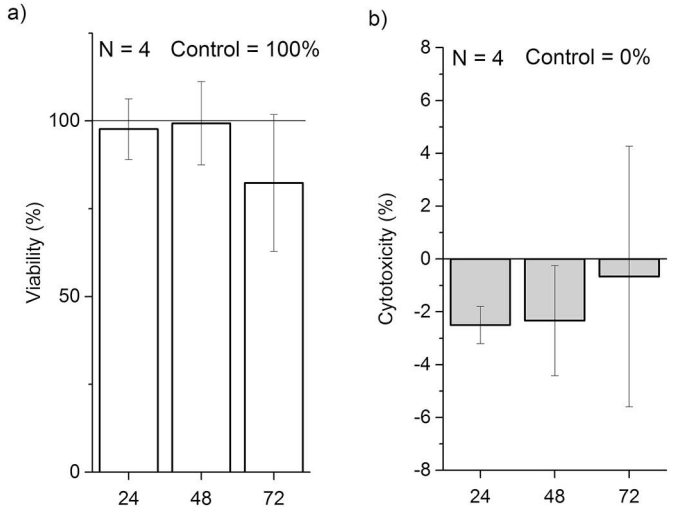

Fig. 15. Cell viability and toxicity of murine macrophages RAW 264.7 cultivated on CoCrMo in RPMI-1640 for 24, 48 and 72 h. The control corresponds to cells cultivated in petri dishes without CoCrMo alloy. The data were analysed using one-way ANOVA: $p = 0.66$ for the viability test and $p = 0.36$ for the cytotoxicity test. The results indicate that there was no significant difference in the viability and cytotoxicity assays with or without CoCrMo.

the viability or induce toxicity.

The number and morphology of cells were monitored by fluorescence microscopy. Fig. 16 presents fluorescent images of the murine macrophages cell line revealed by a lipophilic marker (Test No. 1) and an intracellular pH marker (Test No. 2) during biotribocorrosion tests after the sliding sequences.

The lipophilic marker uniformly highlighted the membrane of the macrophages without difference (Fig. 16 a, b, c). The intracellular pH marker, used during Test No. 2, revealed a majority of weakly blue-labelled cells (pH = 7) with some of them yellowish, indicating an intracellular pH of 4.5–5 (Fig. 16 d, e, f). The green intensity represents acidification in acidic endosomes, lysosomes, and phagosomes.

After accounting for the difference in magnification of the images between the two tests, the cell density was calculated over time. Image processing was performed using ImageJ (binarization, particle area analysis, distribution) to count the number of cells per image surface. The cell density during biotribocorrosion tests is indicated at the bottom of each images. The cell number decreased over time from 50,000 to 29,200 cells/cm^2 for Test No. 1 and from 30,000 to 14,600 cells/cm^2 for Test No. 2. For both tests, the cell density decreased over time. At the end of the friction sequence (5–7 h), only half of the cells that were initially cultured are counted.

Morphological analysis was performed based on the fluorescent images (Table 3). The average cell surface area for Test No. 1 increased from 109 to 165 μm^2 over time, unlike for Test No. 2, where it decreased from 126 to 88 μm^2. The variation in size was not statistically

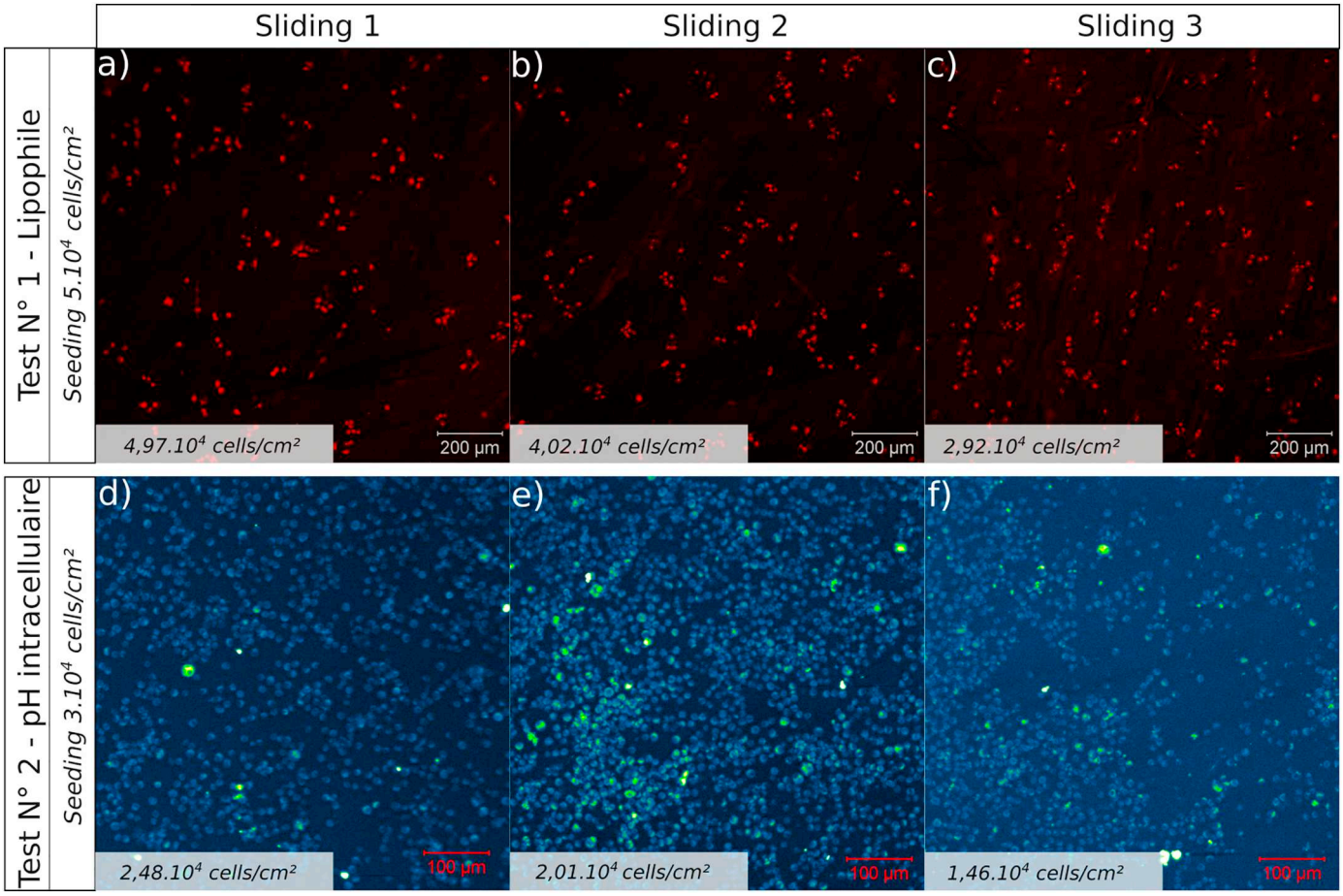

Fig. 16. Fluorescence microscopy images from the living macrophages cultured in Petri dish discs placed around CoCrMo after sliding sequences of biotribocorrosion. The cells were stained to reveal lipids membranes for Test No. 1 (a, b, c) and intracellular pH, which indicates an acidic pH (4.7–5) for a yellow green signal, for Test No. 2 (d, e, f). Note the difference in magnification between the tests. (For interpretation of the references to colour in this figure legend, the reader is referred to the web version of this article).

Table 3
Mean area of macrophages cell lines after the three sliding sequences of the biotribocorrosion tests. The data were analysed using one-way ANOVA followed by a multiple comparison test: p = 0.13 by comparing the three sliding sequences for Test No. 1 and p = 0.002 for Test No. 2, and [a]$p < 0.1$ and, [b] $p < 0.05$ compared between tests.

	Test	Slid. 1[a]	Slid. 2[b]	Slid. 3[b]	Significance
Cell mean area (μm^2)	No. 1	109.2 ± 2.2	143.1 ± 2.6	165.7 ± 3.2	p = 0.13
	No. 2	126.7 ± 1.9	112.1 ± 1.7	88.5 ± 1.3	p = 0.002

different for Test No. 1 ($p = 0.13$) as opposed to for Test No. 2 ($p = 0.002$). The frequency distribution of macrophages for Test No. 1 was similar (from 0 to 400 μm^2), and the range of cell sizes for the three sequences was narrow (results not shown). The cells after the third sliding sequence were comparatively larger (190–310 μm^2) than those after sliding 1 and 2, and had a greater range of cell sizes. More small cells (< 10 μm^2) were present after sliding 1 (28%) than after sliding 2 (8%). The sizes of the macrophages after the first sliding of Test No. 2 were not statistically different from one another ($p = 0.10$), but were different from those after the second and third sliding ($p < 0.05$). More small cells, with an area smaller than 110 μm^2, were present at the end of the test, representing 88% (results not shown).

To determine the inflammatory response of the murine macrophages cell line to polyethylene wear debris and metal ions, the production of prostaglandin E_2 was measured using ELISA. As observed in Table 4, both conditions of Test No. 1 and 2 increased PGE_2 production compared with the control (55.18 pg/ml), however the difference was not statistically significant ($p > 0.1$). Murine macrophages subjected to biotribocorrosion test No. 2 produced 2.5 times more prostaglandin E_2 than initially (140.89 pg/ml). The two tests were not significantly different ($p = 0.30$).

5. Discussion

Based on biocompatibility studies of orthopaedic prostheses indicating the differences between simulated degradation products and those extracted from tissues (size, nature or quantity), we attempted to improve an existing tribometer. Specifically, we produced degradation products from the CoCrMo/PE couple in direct contact with macrophages. We assumed that the applied conditions might generate mainly one type of degradation product over another (polyethylene particles or metal ions). The focus of the study was on the degradation products generated and their effect on the cellular response of macrophages. The following discussion is based on the preliminary results presented in this paper; it is clear that more assays are necessary to confirm the tendencies described below.

5.1. Metal Ion Generation

For both biotribocorrosion tests, the mean potential E_{OCP} of CoCrMo in supplemented RPMI-1640 medium fluctuates in the passive domain range (Fig. 6, Fig. 7, Fig. 8). The UHMW-PE pin acts as a flexible and soft pin rather than as a grinding pin, such as the hard alumina pin used in many studies [70–73]. Using an alumina pin to simulate knee or ankle contact could lead to overestimation of the tribocorrosion of joint prostheses. However, the dissolution of the CoCrMo alloy differed for the two tests performed in this study, which is explained by the different surface conditions and sliding velocities. It is essential to recall that the sample from Test No. 1 had a higher roughness (manual polishing with dry paper *vs.* the mirror polishing used for sample No. 2). This difference is reflected in the corrosion properties of the CoCrMo alloy, which were evaluated by monitoring the evolution of the OCP. The dissolution mechanisms of the CoCrMo alloy, generating metal ions, appeared to be different for these two tests:

- For Test No. 1, the potential of CoCrMo was approximately −250 mV/SCE, which corresponds to the pre-passive range of CoCrMo in RPMI-1640 medium (Fig. 7). The slow evolution of the E_{OCP} (from −250 to −150 mV/SCE) during the friction test suggested that the protective quality of the passive film increases over time. Under friction, there was no evidence (potential drop and transient) of mechanical removal of the passive film because the friction speed was too low to record some passive film removal. The similar rate of Co ion production and low Cr ion increase in the medium compared with the control (Fig. 9) also indicates that the passive film was weakly affected by the mechanical wear and that the maintenance mechanism of the passive film was similar. The experimental conditions in Test No. 1 appear to favour chemical wear at the expense of mechanical wear.
- For Test No. 2, the initial corrosion potential was higher (between −100 and 300 mV/SCE) and decreased over time (Fig. 8). This result suggests that the CoCrMo in sample No. 2 was more passivated in its initial state and then underwent depassivation. The discrepancy with the results for Test No. 1 can be explained by the previously mentioned surface condition difference: the fineness and uniformity of the polishing of CoCrMo of Test No. 2 induces a higher reactivity of the material. Immediately after polishing, the sample stored in air exhibited a native oxide layer that was more homogeneous than that grown on a *SiC* polished surface. Immersed in the solution, the E_{OCP} characterizes the reactivity of the passivated surface with more noble values. However, this passive film appeared to be more sensitive to external stresses, especially after sliding under the pin. The breakdown of the passive film was characterized by a transient in the E_{OCP} curve.

Table 4
Analysis of PGE_2 in supernatants in biotribocorrosion tests using the ELISA technique. The control corresponds to the cells immersed in the supplemented RPMI-1640 medium. The data were analysed using one-way ANOVA followed by a multiple comparison test. [a]p = 0.10 compared with control, [b]p = 0.18 compared with control and p = 0.30 by comparing both tests.

	Control	Test No. 1	Test No. 2
Prostaglandin E_2 (pg/ml)	55.18	100.65[b]	140.89[a]

The increased levels of metal ions (Co, Cr, Mo) measured after ICP-MS analysis (Fig. 9) confirmed that low dissolution accelerated by friction and depassivation occured for Test No. 1 and 2, respectively. Depassivation favours more chromium ions (Cr^{3+}) and molybdenum ions (Mo^{4+}) than cobalt ions (Co^{2+}) because the passive film of CoCrMo is mainly composed of Cr_2O_3 [74]. The molybdenum level, which was higher for Test No. 2, is precisely involved in the reconstruction and repair processes of the passive film, confirming some ruptures in the passive film, as mentioned before. The biotribocorrosion Test No. 2 would further promote the depassivation of the passive film by friction of the polyethylene pin, resulting in a higher metal ion concentration in supplemented RPMI-1640 than in Test No. 1. The mirror-polished surface appeared to be more sensitive to tribocorrosion than *SiC* polished surface. The difference in overall reactivity (evolution of the OCP) between the two tests appears to underline the role of the surface roughness and sliding velocity in the reactivity of the CoCrMo

subjected to biotribocorrosion tests and consequently on the rate of metal ion release into the environment. This device could highlight the sensitivity to this parameter.

The CSR + Rh sequences correspond to a latency period, where no friction is applied and vertical movements of the pin causes convection movements to promote metal ions dispersion in solution. During these periods, repeated twice, the surface reactivity of the two samples was not the same:

- In Test No. 1, these sequences resulted in a significant increase in potential from 400 to 500 mV, which reflects the reactivity of the CoCrMo/RPMI-1640 interface. The potential increase can be attributed to faradic reactions, relative to oxidation-reduction (material and electrolyte) and non-faradic reactions, where no electron transfer but only charge/discharge of the double layer occur [75–78]. When friction stops, the double layer is likely readjusted by the charge effect. This phenomenon is accompanied by the surrounding contribution of the electrolyte to the contact surface released by the pin. The influx of new chemical species such as proteins and dissolved oxygen confers a higher oxidizing power to the solution and thus accelerates the surface reactivity. The structure of the double layer and the specific adsorption of ions affect the kinetics of the electrode processes, resulting in a change in the potential. The large amplitude of the OCP peaks during the CSR + Rh sequence can be explained by the agitation of the solution by acceleration of the charge effects and the solution contribution. Finally, the hydrodynamic and chemical conditions of the solution play decisive roles in the reconstruction of the film.
- The potential curve of Test No. 2 does not vary between the sliding and CSR + Rh sequences. As mentioned previously, cobalt exposes a well-constructed passive film on the surface. From an electrochemical viewpoint, it mainly contributes to interfacial phenomena between the material and solution and has a capacitive behaviour. Reactions involving solvated ions in the double layer are not directly accessible because of the shielding power of the film. The measure of OCP does not allow access to the double layer if the passive film is well developed. The metal alloy appears to be less exposed because of the presence of passive film. Thus, the oxidizing power mentioned above would be mitigated by the presence of this film. In addition, the CoCrMo sample is always constrained during rheology, which locally does not modify the solution as much, *i.e.* the double layer and surface released by the pin are more restricted.

Finally, in this study, corrosion accelerated by wear was a minor phenomenon with a UHMW-PE /CoCrMo contact. This finding is consistent with the fact that dissolution contributing to wear is marginal. It was evaluated at 10% on CoCrMo in physiological fluid [76]. Finally, for the rheology phase, it would be useful to evaluate the non-faradic reactions with low sliding displacement (0.6 mm/s).

5.2. Polymeric Wear Debris Generation

One of the particularities of the biotribocorrosion set-up is that it allows the generation of both ions and polyethylene wear debris in the same environment. The wear mechanism of the polyethylene/CoCrMo alloy contact was evaluated by examining the variation of the friction coefficient during sliding; the wear volume of UHMW-PE; and the shape, nature and distribution of the polyethylene wear particles.

For both biotribocorrosion tests, a low friction coefficient was measured (< 0.12), suggesting that the UHMW-PE/CoCrMo couple operated under boundary lubrication (Fig. 10). The decrease of the friction coefficient values is dependent on the characteristics of the lubricant and especially of the proteins. In supplemented RPMI-1640, proteins are present at 6.18 g/l. They are most likely adsorbed on the metal surface, forming a layer at the nanoscale that is driven by the physico-chemical properties of the surface [79]. Under tribological contacts, previous studies have shown that proteins lubricate the surface of materials by forming a complex film and thus significantly reduce the COF [23,80,81]. These results are consistent because the RPMI-1640 is a biological medium that is rich in organic compounds. However, large molecules (hyaluronic acid and albumin) could form rollers containing lipids on the surface, filling the space between the first bodies and increasing the friction coefficient [82]. We assumed that this difference results from the competitive adsorption (Vroman effect [83]) between organic molecules in terms of dynamics and conformation. Small molecules preferentially adsorb on the surface before large, less mobile ones.

Although the amplitude and distribution of contact pressure can affect wear rates, we compared the wear volumes in this study with those determined from similar previous data [41,84–86]. The wear volumes of UHMW-PE determined in this study were consistent with those reported in previous studies involving 1050 UHMW-PE, ranging from 1.2 to 17.8 mm^3/MC. The discrepancy between the results for the two tests in this study can be explained by the surface conditions of the CoCrMo *i.e.*, the roughness. In a polymer/metal contact, wear is assumed to mainly affect the polymer component, which is softer than the metal component. Adherence sites result in a higher wear rate of the counter. Therefore, Test No. 1, with a rougher cobalt surface, promotes adhesive wear. The accumulation of polyethylene wear particles in the wear track is consistent with the predominant wear mechanism (Fig. 12). In contrast, the smooth surface of cobalt in Test No. 2 appears to promote abrasive wear, and the third body would act more as a lubricant. Wear debris are trapped and crushed in the contact, and limited debris is ejected. Although wear is affected by many factors, these results are consistent with those in the literature, as adhesive wear is the predominant wear mechanism of joint replacements [87].

Fluorescence observation of the polymer wear debris on the contact surfaces and in the solution revealed a large number of round polyethylene particles for Test No. 1 and small fibrillar-shaped particles for Test No. 2. The spherical shape is more consistent with the wear particles retrieved in synovial fluid from well-functioning total ankle arthroplasties [88]. However, previous work has shown that the number of fibril-shaped polyethylene particles increases over time during wear tests [41,89], which could explain the discrepancy in the particle shape between the two tests, which lasted 5 and 7 h. In this study, we collected the polyethylene wear particles, without further digestion processes because previous studies have shown that complex digestion processes lead to changes in the physicochemical characteristics, of isolated wear particles [90]. However, the synthesized wear particles were most likely surrounded by a thin layer of protein or cellular debris, which can cause a differential response in cellular toxicity.

5.3. Cytotoxicity of Degradation Products and Clinical Concern

5.3.1. Viability of Macrophages

In situ observation of living macrophages during biotribocorrosion tests provides additional information on the cell viability, as fluorescent images enable determination of the cell viability by monitoring changes in the cell density, mean cell surface distribution, and specific markers of the inflammatory response (Fig. 16). In this study, the cell density decreased by nearly half after 5–7 h, suggesting that the degradation products generated (ions and debris) significantly and negatively affected cell proliferation. Preliminary viability/cytotoxicity tests (MTT and LDH) of macrophages on CoCrMo for 72 h indicated that the cytotoxicity does not originate from the material itself but most likely from the degradation products generated during the biotribocorrosion tests (Fig. 15). The cellular conditions (temperature and carbon dioxide levels), which were kept stable throughout the tests, were not considered to be a decisive disruptive element in the proliferation. Moreover, cytotoxicity values are $< 5\%$ indicates that the possibility of contamination from dirty material is negligible. No traces have been visually detected and the LDH test is recognized as a very suitable test

to detect cytotoxicity. The LDH test rejects the existence of contamination.

The macrophages behaved differently in the two biotribocorrosion tests performed: their average surface area increased, *i.e.* they spread over the support surface and favoured their attachment point in Test No. 1, whereas their average surface area decreased during test No. 2, which implies shrinkage. In general, monocytes strongly adhere to most surfaces initially, however, a disruption of adhesion signals can promote cell detachment and induce apoptosis [91]. Moreover, the topography of the alloy surfaces has a direct effect on the adhesion and activation levels of macrophages. Previous studies have shown that macrophage adhesion increases on rough surfaces compared with that on smooth surfaces, because of the increase in the number of adhesion points [92]. The decrease in macrophage adhesion in Test No. 2 may have resulted from both the smooth metal surface, which reduced the number of adhesion points, and the effect of wear debris on the adhesion signals. The cell shape characteristics may be related to their phagocytic capacities. Some authors have suggested a ruffled and irregular cell membrane for pulmonary macrophages after phagocytosis of the particles [93]. The macrophages may have been in a more advanced phagocytosis stage during Test No. 2 than during Test No. 1, which would indicate an inflammatory state that is consistent with the larger amount of debris analysed. Cell shape changes have also been associated with different functional states of cells (proliferation and apoptosis), nuclear organization, cell differentiation, and muscle cell contractility. Even if the surface characteristics could not be visualized at the selected magnification, the restriction in surface area of cells exposed to Test No. 2 indicates a degree of cellular damage [94].

The final point was corroborated by analysis of prostaglandin E_2 in supernatants (Table 4). The measured PGE_2 level was 2–2.5 times higher for both biotribocorrosion tests than for the control, suggesting that PGE_2 is sensitive to all the generated degradation products (polyethylene debris and ions). The measured amount of PGE_2 was normalized by the total amount of proteins released into the extracellular medium and therefore by the number of cells, facilitating comparison. It has been postulated that the phagocytosis of wear particles and metal ions can activate macrophages, causing the release of several inflammatory mediators (TNF-α, IL-1β, IL-6, PGE_2) that have the potential to stimulate bone resorption. Shanbhag et al. [95] and Voronov et al. [55] have demonstrated an increase in the production of PGE_2 in response to exposure to submicron polyethylene particles. Shrivastava et al. [96] also demonstrated that macrophages with Co and Cr ions led to the release of TNF-α and PGE_2. The variance in cytokine response between the two biotribocorrosion tests in this study can be explained by the same reason mentioned above, where the soluble nature of ions has a more rapid effect on cellular metabolism. PGE_2 synthesis appears to be sensitive to exposure to degradation products, and is both dose-dependent and product-composition-specific [97]. This study suggests that, when exposed to both polyethylene wear debris and metal ions, murine macrophages tend to be more affected by metal ions owing to their easier internalization by endocytosis, increasing their cytotoxic character. However, because of the lack of reproducibility of the tests, the cytokine analyses were not significantly different for the control and the two tests ($p > 0.1$). The above conclusions are thus assumptions that remain to be confirmed.

Numerous factors may affect macrophage cell line behaviour near CoCrMo surfaces, including the current distribution created by the position of the counter electrode around the metallic sample and the interaction of this current with the bioelectric properties of the cell surfaces and membranes. Previous works have shown that a bioelectric field can induce reversible permeability (electroporation) or event apoptosis of cells [98,99]. It is clear that the disposition of the electrodes can induce current distributions and thus macrophage viability. Future tests should be performed to determine the extent to which electrochemical assembly may compromise biological results.

5.3.2. Clinical Relevance of Degradation Products

The two distinct behaviours in cell morphology observed in this study can be explained by the nature of the degradation products in the biotribocorrosion tests. As mentioned above, Test No. 1 generates more polyethylene wear debris than Test No. 2, which promotes the dissolution of metal ions. Because of their soluble forms, metal ions are easily evacuated in solution and then react faster on macrophages metabolism than polyethylene wear debris. The critical factors governing the cytotoxicity of degradation products differ depending on whether the products are debris or ions. The biological reactivity of wear debris on macrophages depends on the shape and size of the debris more than on its concentration, whereas the cytotoxic character of metal ions depends on the nature of the ions and mainly on their concentration [100].

The results of ICP-MS analysis indicated that chromium ion were significantly the main product of the dissolution of CoCrMo during Test No. 2. At equal concentrations, chromium is known to induce the greatest inflammatory response followed by cobalt, nickel and molybdenum [3,5]. The results of Test No. 2 suggest that metal ions, and especially chromium ions, are mainly responsible for the cellular damages due to their nature, concentration and mobility in the physiological fluid. It is difficult to directly compare clinical data of metallic ion concentration with that obtained in biotribocorrosion tests. However, a previous study reported concentrations of up to 2 ppm Co and 12 ppm Cr measured in tissues around CoCr devices from revision of total hip replacements [101], whereas another study reported higher concentrations of up to 67 ppm Co and 260 ppm Cr [102]. These concentrations are very high compared with the conditions simulated in this study and could explain the modest variations in cellular behaviour. The discrepancy is mainly attributed to the exposure time, which was underestimated in our study compared with the tissues analysed. In addition, *in vivo* metal ions can be easily transported out of a joint contact, significantly reducing the concentration in the tissues surrounding the implant. In this study, in which the system was closed, the concentration can increase rapidly. Therefore, metal ions directly originating from tribological sites (as in this study) can accumulate in high doses and lead to highly toxic conditions, which are far from clinical or real conditions. Determination of the exact mechanisms responsible for the cytotoxic character of metal ions on murine macrophages would require further assays. Based on previous works, metal ions would most likely stimulate a hypersensitivity response, induce the oxidation of cytoplasmic proteins [35], create an oxidative stress, and activate the secretion of pro-inflammatory cytokines that generate osteolysis of metal implants [5,40,103]. Our data suggest that at clinically relevant levels, macrophages are subjected to chromium release (Cr^{3+} or Cr^{6+}) that is highly toxic to local bone cells in the prosthesis microenvironment, leading to several clinical implications for local bone health. The suppression of osteoblast activity may explain early aseptic release as a failure of primary osseointegration. Cell co-culture assays could be considered to elucidate the synergistic effects of ions and pro-inflammatory cytokines on bone cells.

Macrophages are present at significantly higher concentrations in osteolysis areas and are responsible for bone loss in osteolytic lesions. Exposure of implant wear particles to macrophages is known to result in the release of inflammatory cytokines and activation of the RANKL pathway. Macrophages have been shown to react with polyethylene particles, which are small enough to undergo phagocytosis (0.3–10 μm) [54,104], with those between 0.1 and 1 μm in size being the most reactive [2,6]. Larger particles cause little inflammatory reaction and are therefore unlikely to stimulate osteolysis [105]. The results of the two biotribocorrosion tests in this study suggest that the smallest particles (16.6 μm) affect the viability of macrophages more than larger particles (Fig. 14). The size of wear debris collected in peri-prosthetic tissues range from submicron levels to 100 μm [88], which corresponds well to the size of the particles generated in this study. It is particularly interesting to note that the number of particles in Test No. 2 (5541) was

three times less than that in Test No. 1 (14,394), but led to higher cytotoxicity on macrophages (Fig. 13, Table 3). Other studies have already shown that size and shape (but not quantity) of wear debris are some of the major factors determining cytotoxicity on monocyte-like cells. A smaller volume of more active debris is essentially equivalent to a larger volume of fibrillary-shaped debris.

Polymer particle shape is also thought to be an important factor determining tissue reaction and osteolysis. The particles characterized from the peri-prosthetic tissues of retrieved implants were round, oval, needle-shaped, and spike-shaped [106,107], corresponding to the shapes of the polymer wear debris generated in this study (Fig. 13). However, there are still disparities in the analysis of the physico-chemical characteristics of wear particles and degradation products of tissue samples in different studies, which result from the variation in the isolation methods used by researchers [43–45]. This study makes it possible to avoid these controversies, and it is therefore possible to consider that the polymer wear particles from these biotribocorrosion tests are not too different in size from the debris produced *in vivo*. However, further studies are needed to confirm these statements. It has also been demonstrated that a rough surface and fibrillary shape leads to increased cytokines production compared with a smooth surface and globular shape [108,109], which is consistent with the fluorescence image analysis of macrophages revealing more cytotoxicity during Test No. 2 in the current study (Fig. 16). The roll-shaped and fibrillar particles may stimulate a greater inflammatory reaction of surrounding macrophages over time than round particles produced during Test No. 1 (Fig. 11 and Fig. 13). Polyethylene wear debris are associated with an immune response that triggers osteolysis and aseptic loosening [110–112].

Because the metal ions were much more concentrated in Test No. 2, it is possible that they acted in accordance with the particles. Indeed, metal ions embedded in polyethylene particles [113] can act as catalysts, increasing the rates of oxidation and changing the particle surface chemistry. The oxidized particles could result in enhanced cellular activation to compare with non-oxidized particles. Within the time frame of Test No. 1, the absence of fluorescence variability over time may also be due to either a lack of sensibility or too short of contact time between the debris and macrophages. The form of cell death and the release of pro-inflammatory cytokines appears to be time-dependent [100]. An incubation time of at least 24 h would determine whether it is time dependent.

Moreover, because of the smaller size of metallic nanoparticles relative to microparticles, they can also be dissolved in fluids, leading to more impairment in phagocytosis and increased toxicity to macrophages. In this study, the underestimation of nano- and micro-CoCrMo particles present in the medium could further explain the differences from the results of other *in vitro* studies. These particles could contribute to toxicity, as small particles can be phagocytosed more frequently and more rapidly than larger particles. Particles can also be dissolved, therefore, the total ions levels depend on the residence time and their location in the human body [40,103]. Particles are is therefore of importance even though it is difficult to extract them from periprosthetic tissues without dissolving them.

5.4. Effect of Multiple Parameters

The experimental conditions used in the different biotribocorrosion tests differ in terms of the mechanical parameters (CoCrMo roughness, sliding velocity, loading during rheology sequence), biological parameters (fluorescent marker, cell density), and test duration. The synergistic effects between these factors are difficult to consider at the same time. Therefore, the variation of mechanical parameters was mainly discussed during the establishment of the wear mechanisms and surface reactivity. The biological parameters and roughness of CoCrMo were addressed during the cellular study. The duration of the tests was taken into account both for the cellular response and the degradation processes of the materials (shape of polyethylene wear debris). Synergistic effects may occur between these multiple factors, with further work required to identify them.

6. Limitations

Although the proposed biotribocorrosion set-up provides a multidisciplinary approach to examine contact joint durability, there are several important limitations inherent to this study.

Temperature variations, even of less than 1 °C, can significantly affect the focus of fluorescence images of cells [114]. Therefore, temperature control of the microscope should be provided. Some highly reactive chemicals, products of the photobleaching process (also termed fading), can also interfere with cellular processes. It is therefore important to minimize light exposure to preserve both the fluorescence signal and normal cellular activity [114].

Short-term testing (7 h) may underestimate long-term cumulative toxicity responses and therefore overestimate tolerable thresholds *in vivo*. Longer duration tests are required to elucidate the relationship between the particle quantity and clinical outcomes over medium- and long-term monitoring. The dissolution rate of joint prostheses with CoCrMo/polymer contact must also take into account active and passive periods of stress to simulate daily activities.

Similarly, the tribological system does not take into account the evolution of load over time. Biotribocorrosion tests were performed using a pin-on-flat contact, which may not reflect the applied tibiotalar kinematics *in vivo*. The ankle joint mechanics include dorsiflexion and plantar flexion, which could induce a higher wear rate and generate dissimilar wear debris. For an ankle prosthesis, the mechanical forces exerted vary depending on the gait cycle. The absence of a dynamic force cycle is one of the limitations of this study. In addition, the experiments were performed with an applied force of 35 N, resulting in a contact stress of 25 MPa, which is in the load range calculated for ankle replacement. However, the peak contact pressure is dependent on the prosthesis model: Agility ranges from 26 to 36 MPa, that for BOX is between 10.3 and 16.1 MPa and STAR has a contact pressure greater than 20 MPa [65]. Stack et al. performed one of the few works with very low loads on a Co-Cr/UHMWPE couple [37]. They showed that at low loads (0.5–3 N) and anodic potentials, corrosion prevails over abrasion. This finding is consistent with our results because the abrasion was relatively low. Therefore, the relevance of this study lies in the use of low contact stress, as other tribocorrosion studies have been performed under higher contact stress (800–1270 MPa) because of the applied load and geometry of the counter body [71,115]. Future work should focus on tests that can apply a load/discharge simultaneously with the friction movement, with an initial contact pressure that can reach 100 N, to study different friction torques simulating different joint prostheses.

Our preliminary studies show that polymer wear debris produced directly in cell culture medium, significantly affect the proliferation and inflammatory response of macrophages. Although no specific assays of metal nanoparticles were performed, it is clear that the cells could also be affected by their cytotoxic character [57]. Clearly, further studies are needed to determine the amount of metal nanoparticles produced, as these nanoparticles are likely to form *in vivo* upon mechanical abrasion of the implant oxide film surface.

It is important to note that there are many differences between the biological environment and current experimental conditions. The solution used was not as simple as that typically used (0.9% NaCl); however, compared with the synovial fluids present in the human body, the solution remains simplified. It is known that proteins contained *in vivo*, such as macrophage inflammatory protein (MIP)-1, can increase inflammatory effects. Proteins also act as limiting lubricants that reduce friction, and thus wear on the metal surface. Upon deposition on the surface of the metal, proteins form a carbonaceous layer with ions and salts known as tribolayer [80,116,117] with a protective nature

[53,116]. The protein adsorption could **i)** modify the stable growth of a protective oxide film, **ii)** limit oxygen diffusion for repassivation [118], and/or **iii)** reduce mechanical stimulus by lubrication. These factors could explain the low ionic dissolution of CoCrMo exposed to biotribocorrosion tests in RPMI-1640 because the adsorption of organic compounds, such as proteins, occurs in the passive domain of CoCrMo alloys [119]. Thus, a simulated medium similar to the synovial fluid, such as the biomimetic fluid developed by Sava et al. [58], and ideally in which cells can proliferate [120], should be used in future work.

The *in vitro* study used murine cell lines that can only approximate human conditions and cells *in vivo*. Generally, established cell lines are more resilient than primary cells and therefore represent a conservative upper limit of tolerable conditions for these cell types. Previous studies have shown that established cell lines can be two to three times more tolerant to the exposure of CoCrMo alloy particles than primary cells [121]. Human macrophages, such as the SC cell line from ATCC (CRL-9855) should preferably be used for further clinical transfer in future work.

One of the limitations of this study is the lack of repeatability of the biotribocorrosion tests. As mentioned above, this study presents preliminary results to demonstrate the potential of the designed experimental system. However, it is clear that further testing is required to support the current assumptions and conclusions. Specifically, the bioassays should at least be performed in triplicate and supplemented by targeted analyses of pro-inflammatory cytokines.

7. Conclusion

The aim of the present study was to develop a biotribocorrosion set-up, based on an existing tribometer, to simulate the physiological conditions of a prosthetic joint contact. The main advantage of the proposed system is the ability to simultaneously perform tribological, electrochemical and biological analyses in an environment adapted to cell culture. Degradation products generated by UHMW-PE/CoCrMo alloy contact (metal ions and polymer wear debris) were evaluated, and their toxicity on living murine macrophages was examined. Our preliminary results suggest that two types of degradation mechanisms (ionic and adhesive wear) can be promoted depending on the experimental conditions (roughness and sliding velocity), which implies the presence of either polyethylene wear particles or metal ions. These findings indicate that the degradation products generated by the biotribocorrosion set-up, which attempts to mimic *in vivo* conditions, could be considered as a model system to study the toxicity of degradation products on cells without the need to use ionic salts or commercially available model wear particles. Our *in vitro* results suggest that metal ions induce a higher inflammatory response on macrophages than polymer wear debris, because of their mobility and soluble state. This multidisciplinary study suggests the need to simultaneously test clinically relevant doses of wear particles and ions and to further investigate the cellular response over the long term.

Authors' contributions

A.I. conceived, planned, and performed the experiments, performed the analysis and processed the experimental data. A.I. and A.M.S. conceived the original biotribocorrosion device. A.I. wrote the manuscript and designed the figures with support from A.M.S. and B.N. B.T.O., C.D.L., and A.B.B. aided in interpreting the electrochemical and tribological results. L.B. and S.M. contributed to the interpretation of the biocompatibility results. B.N. and Y.B. supervised the project. All the authors provided critical feedback and helped shape the research, analysis, and final manuscript.

Acknowledgments

The design and manufacture of the bio-tribometer was supervised by Ana-Maria Trunfio-Sfarghiu under a grant from the French National Research Agency “Biolub” (ANR Blanc SIMI 4: 2012-2016). Adaptation of the biotribocorrosion set-up configuration as well as the purchase of all of the consumables necessary for this study was supported by a grant from INSA Lyon (BQR 2016-2018), supervised by Christelle Der-Loughian and Aline Bel-Brunon, and from Carnot Institute Ingénierie@ Lyon (TROPISME project). The authors would like to thank David Levèque for his contribution to the Biolub software development, Romain Trunfio for his assistance in machining parts for the biotribocorrosion set-up, Carole Bougault and Marwa Ben Braham for performing the inflammatory reaction analyses, and Philippe Telouk for the ICP-MS analyses. Tornier provided the UHMW-PE samples. Finally, the authors would like to thank all the trainees who participated in this project during their master's degree: Lénaïg Colliot, Pierre Le Saout and Joris Carmona.

References

[1] J.L. Besse, Osteolytic cysts with total ankle replacement: frequency and causes? Foot Ankle Surg. 21 (2015) 75–76, https://doi.org/10.1016/j.fas.2015.03.005.
[2] Van Citters, 14 - Failure analysis of orthopaedic implants, Wear of orthopaedic implants and artificial joints (2013) 377–402, https://doi.org/10.1533/9780857096128.1.377.
[3] M.S. Caicedo, R. Desai, K. McAllister, A. Reddy, J.J. Jacobs, N.J. Hallab, Soluble and particulate Co-Cr-Mo alloy implant metals activate the inflammasome danger signaling pathway in human macrophages: A novel mechanism for implant debris reactivity, J. Orthop. Res. 27 (2009) 847–854, https://doi.org/10.1002/jor.20826.
[4] Joshua J. Jacobs, N.J. Hallab, A.K. Skipor, R.M., Urban, metal degradation products: a cause for concern in metal-metal bearings? Clin. Orthop. Relat. Res. (2003) 139–147, https://doi.org/10.1097/01.blo.0000096810.78689.62.
[5] K. Magone, D. Luckenbill, T. Goswami, Metal ions as inflammatory initiators of osteolysis, Arch. Orthop. Trauma Surg. 135 (2015) 683–695, https://doi.org/10.1007/s00402-015-2196-8.
[6] E. Ingham, J. Fisher, The role of macrophages in osteolysis of total joint replacement, Biomaterials. 26 (2005) 1271–1286, https://doi.org/10.1016/j.biomaterials.2004.04.035.
[7] D.W. Murray, N. Rushton, Macrophages stimulate bone resorption when they phagocytose particles, J. Bone Joint Surg. (Br.) 72 (B) (1990) 988–992.
[8] G.J. Atkins, D.R. Haynes, D.W. Howie, D.M. Findlay, Role of polyethylene particles in peri-prosthetic osteolysis: a review, World J. Orthop. 2 (2011) 93, https://doi.org/10.5312/wjo.v2.i10.93.
[9] A.M. Kandahari, X. Yang, K.A. Laroche, A.S. Dighe, D. Pan, Q. Cui, A review of UHMWPE wear-induced osteolysis: the role for early detection of the immune response, Bone Res. 4 (2016) 1–13, https://doi.org/10.1038/boneres.2016.14.
[10] H.-G. Willert, H. Bertram, G.H. Buchhorn, Osteolysis in Alloarthroplasty of the hip, Clin. Orthop. Relat. Res. (1990) 108–121, https://doi.org/10.1097/00003086-199009000-00013.
[11] I. Catelas, A. Petit, H. Vali, C. Fragiskatos, R. Meilleur, D.J. Zukor, J. Antoniou, O.L. Huk, Quantitative analysis of macrophage apoptosis vs. necrosis induced by cobalt and chromium ions in vitro, Biomaterials 26 (2005) 2441–2453, https://doi.org/10.1016/j.biomaterials.2004.08.004.
[12] S.S. Jakobsen, G. Danscher, M. Stoltenberg, A. Larsen, J.M. Bruun, T. Mygind, K. Kemp, K. Soballe, Cobalt-chromium-molybdenum alloy causes metal accumulation and metallothionein up-regulation in rat liver and kidney, Basic Clin. Pharmacol. Toxicol. 101 (2007) 441–446, https://doi.org/10.1111/j.1742-7843.2007.00137.x.
[13] D. Cadosch, E. Chan, O.P. Gautschi, L. Filgueira, Metal is not inert : role of metal ions released by biocorrosion in aseptic loosening - current concepts, J. Biomed. Mater. Res. A 91 (2009) 1252–1262, https://doi.org/10.1002/jbm.a.32625.
[14] R. Pandey, J. Quinn, C. Joyner, J.T. Mdw, N.A. Triffiti, Athanasou, Particles of biomaterials recruit macrophages which can differentiate into bone resorbing cells, Adv. Mater. Sci. Implant Orthop. Surg. 294 (1995) 13–24.
[15] S. Ramakrishna, M. Ramalingam, T.S.S. Kumar, W.O. Soboyejo, Failure and Tribology of Biomaterials, in: Biomater. a Nano Approach, CRC Press, 2010, pp. 81–121.
[16] S. Goodman, Wear particulate and osteolysis, Orthop. Clin. North Am. 36 (2005) 41–48, https://doi.org/10.1016/j.ocl.2004.06.015.
[17] F.G. Krause, M. Windolf, B. Bora, M.J. Penner, K.J. Wing, A.S.E. Younger, Impact of complications in total ankle replacement and ankle arthrodesis analyzed with a validated outcome measurement, J. Bone Jt. Surg. 93 (2011) 830–839, https://doi.org/10.2106/JBJS.J.00103.
[18] M.A. Glazebrook, K. Arsenault, M. Dunbar, Evidence-based classification of complications in Total ankle arthroplasty, Foot Ankle Int. 30 (2009) 945–949, https://doi.org/10.3113/FAI.2009.0945.
[19] Y. Takakubo, A. Berce, R. Trebše, Y. Tamaki, I. Milošev, A. Al-Samadi, V.-M. Tiainen, Y.T. Konttinen Orton, Wear and corrosion in the loosening of total joint replacements (TJRs), Bio-Tribocorrosion Biomater, Woodhead Publishing Limited, Med. Implant, 2013, pp. 74–110, , https://doi.org/10.1533/9780857098603.1.74.
[20] Y. Yan, D. Dowson, A. Neville, In-situ electrochemical study of interaction of

tribology and corrosion in artificial hip prosthesis simulators, J. Mech. Behav. Biomed. Mater. 18 (2013) 191–199, https://doi.org/10.1016/j.jmbbm.2012.08.009.
[21] B. Alemón, M. Flores, W. Ramírez, J.C. Huegel, E. Broitman, Tribocorrosion behavior and ions release of CoCrMo alloy coated with a TiAlVCN/CNx multilayer in simulated body fluid plus bovine serum albumin, Tribol. Int. 81 (2015) 159–168, https://doi.org/10.1016/j.triboint.2014.08.011.
[22] A.W.E. Hodgson, S. Kurz, S. Virtanen, V. Fervel, C.O.A. Olsson, S. Mischler, Passive and transpassive behaviour of CoCrMo in simulated biological solutions, Electrochim. Acta 49 (2004) 2167–2178, https://doi.org/10.1016/j.electacta.2003.12.043.
[23] M.J. Runa, M.T. Mathew, M.H. Fernandes, L.A. Rocha, First insight on the impact of an osteoblastic layer on the bio-tribocorrosion performance of Ti6Al4V hip implants, Acta Biomater. 12 (2015) 341–351, https://doi.org/10.1016/j.actbio.2014.10.032.
[24] M.A. Wimmer, M.P. Laurent, M.T. Mathew, C. Nagelli, Y. Liao, L.D. Marks, J.J. Jacobs, A. Fischer, The effect of contact load on CoCrMo wear and the formation and retention of tribofilms, Wear 332–333 (2015) 643–649, https://doi.org/10.1016/j.wear.2015.02.013.
[25] M.T. Mathew, M.A. Wimmer, Tribocorrosion in Artificial Joints: In Vitro Testing and Clinical Implications, in: Tribocorrosion Passiv, Woodhead Publishing Limited, Met. Coatings, 2011, pp. 368–400, https://doi.org/10.1016/B978-1-84569-966-6.50013-0.
[26] S. Mischler, A.I. Muñoz, Wear of CoCrMo alloys used in metal-on-metal hip joints: a tribocorrosion appraisal, Wear 297 (2013) 1081–1094, https://doi.org/10.1016/j.wear.2012.11.061.
[27] A.I. Muñoz, J. Schwiesau, B.M. Jolles, S. Mischler, In vivo electrochemical corrosion study of a CoCrMo biomedical alloy in human synovial fluids, Acta Biomater. 21 (2015) 228–236, https://doi.org/10.1016/j.actbio.2015.03.008.
[28] P.A.A.P. Marques, M.C. Magalhaes, R.N. Correia, Inorganic plasma with physiological CO2/HCO3- buffer, Biomaterials 24 (2003) 1541–1548 (S0142961202005392).
[29] A. Ouerd, C. Alemany-Dumont, B. Normand, S. Szunerits, Reactivity of CoCrMo alloy in physiological medium: electrochemical characterization of the metal/protein interface, Electrochim. Acta 53 (2008) 4461–4469, https://doi.org/10.1016/j.electacta.2008.01.025.
[30] M. Haeri, S. Goldberg, J.L. Gilbert, The voltage-dependent electrochemical impedance spectroscopy of CoCrMo medical alloy using time-domain techniques: generalized Cauchy-Lorentz, and KWW-Randles functions describing non-ideal interfacial behaviour, Corros. Sci. 53 (2011) 582–588, https://doi.org/10.1016/j.corsci.2010.09.067.
[31] J.J. Ryu, P. Shrotriya, Mechanical load assisted dissolution response of biomedical cobalt–chromium and titanium metallic alloys: influence of in-plane stress and chemical environment, Wear 332–333 (2015) 662–668, https://doi.org/10.1016/j.wear.2015.01.071.
[32] L.N. Wang, X.Q. Huang, A. Shinbine, J.L. Luo, Influence of albumin on the electrochemical behaviour of Zr in phosphate buffered saline solutions, J. Mater. Sci. Mater. Med. 24 (2013) 295–305, https://doi.org/10.1007/s10856-012-4816-y.
[33] X. Cheng, S.G. Roscoe, Corrosion behavior of titanium in the presence of calcium phosphate and serum proteins, Biomaterials. 26 (2005) 7350–7356, https://doi.org/10.1016/j.biomaterials.2005.05.047.
[34] L. Hongtao, G. Shirong, C. Shoufan, W. Shibo, Comparison of wear debris generated from ultra high molecular weight polyethylene in vivo and in artificial joint simulator, Wear. 271 (2011) 647–652, https://doi.org/10.1016/j.wear.2010.11.012.
[35] A. Petit, F. Mwale, C. Tkaczyk, J. Antoniou, D.J. Zukor, O.L. Huk, Induction of protein oxidation by cobalt and chromium ions in human U937 macrophages, Biomaterials. 26 (2005) 4416–4422, https://doi.org/10.1016/j.biomaterials.2004.11.019.
[36] I. Catelas, R. Vanos, L.L. Lildhar, E.A. Lehoux, P.E. Beaul, *In Vitro* Macrophage Response to Nanometer-Size Chromium Oxide Particles, (2013), pp. 149–159, https://doi.org/10.1002/jbm.b.32991.
[37] M.M. Stack, J. Rodling, M.T. Mathew, H. Jawan, W. Huang, G. Park, C. Hodge, Micro-abrasion–corrosion of a co–Cr/UHMWPE couple in Ringer's solution : an approach to construction of mechanism and synergism maps for application to bio-implants, Wear. 269 (2010) 376–382, https://doi.org/10.1016/j.wear.2010.04.022.
[38] C.G. Figueiredo-Pina, A. Matos Neves, B.M. Bandarra das Neves, Corrosion-wear evaluation of a UHMWPE/Co-Cr couple in sliding contact under relatively low contact stress in physiological saline solution, Wear 271 (2011) 665–670, https://doi.org/10.1016/j.wear.2010.11.014.
[39] D. Tetreault, F. Kennedy, Friction and wear behavior of ultrahigh molecular weight polyethylene on co-Cr and titanium alloys in dry and lubricated environments, Wear 133 (1989) 295–307.
[40] R.E. Andrews, K.M. Shah, J.M. Wilkinson, A. Gartland, Effects of cobalt and chromium ions at clinically equivalent concentrations after metal-on-metal hip replacement on human osteoblasts and osteoclasts: implications for skeletal health, Bone. 49 (2011) 717–723, https://doi.org/10.1016/j.bone.2011.06.007.
[41] O.N. Schipper, S.L. Haddad, S. Fullam, R. Pourzal, M.A. Wimmer, Wear characteristics of conventional ultrahigh-Molecular-Weight Polyethylene Versus Highly Cross-Linked Polyethylene in total ankle arthroplasty, Foot Ankle Int. (2018) 1–10, https://doi.org/10.1177/1071100718786501.
[42] L. Yahia, O.L. Huk, I. Catelas, A. Petit, D.J. Zukor, R. Marchand, Induction of macrophage apoptosis by ceramic and polyethylene particles in vitro, Biomaterials 20 (2002) 625–630, https://doi.org/10.1016/s0142-9612(98)00214-2.
[43] P. Campbell, S. Ma, B. Yeom, H. McKellop, T.P. Schmalzried, H.C. Amstutz, Isolation of predominantly submicron-sized UHMWPE wear particles from periprosthetic tissues, J. Biomed. Mater. Res. 29 (1995) 127–131, https://doi.org/10.1002/jbm.820290118.
[44] M. Slouf, S. Eklova, J. Kumstatova, S. Berger, H. Synkova, A. Sosna, D. Pokorny, M. Spundova, G. Entlicher, Isolation, characterization and quantification of polyethylene wear debris from periprosthetic tissues around total joint replacements, Wear. 262 (2007) 1171–1181, https://doi.org/10.1016/j.wear.2006.11.005.
[45] P. Campbell, S. Ma, T. Schmalzried, H.C. Amstutz, Technical Note. Tissue digestion for wear debris particle isolation, J. Biomed. Mater. Res. 28 (1994) 523–526, https://doi.org/10.1016/B978-0-08-021444-3.50005-7.
[46] M.J. Nine, D. Choudhury, A.C. Hee, R. Mootanah, N.A.A. Osman, Wear debris characterization and corresponding biological response: artificial hip and knee joints, Materials (Basel) 7 (2014) 980–1016, https://doi.org/10.3390/ma7020980.
[47] Y. Yan, A. Neville, D. Dowson, Tribo-corrosion properties of cobalt-based medical implant alloys in simulated biological environments, Wear. 263 (2007) 1105–1111, https://doi.org/10.1016/j.wear.2007.01.114.
[48] A. Kocijan, I. Milošev, D.K. Merl, B. Pihlar, Electrochemical study of co-based alloys in simulated physiological solution, J. Appl. Electrochem. 34 (2004) 517–524, https://doi.org/10.1023/B:JACH.0000021868.10122.96.
[49] A. Kocijan, I. Milošev, B. Pihlar, The influence of complexing agent and proteins on the corrosion of stainless steels and their metal components, J. Mater. Sci. Mater. Med. 14 (2003) 69–77, https://doi.org/10.1023/A:1021505621388.
[50] Y. Okazaki, E. Gotoh, Comparison of metal release from various metallic biomaterials in vitro, Biomaterials. 26 (2005) 11–21, https://doi.org/10.1016/j.biomaterials.2004.02.005.
[51] Y. Hedberg, X. Wang, J. Hedberg, M. Lundin, E. Blomberg, I. Odnevall Wallinder, Surface-protein interactions on different stainless steel grades: effects of protein adsorption, surface changes and metal release, J. Mater. Sci. Mater. Med. 24 (2013) 1015–1033, https://doi.org/10.1007/s10856-013-4859-8.
[52] T. Groth, K. Klosz, C. EJ, R. New, H. B, G. H, Protein adsorption, lymphocyte adhesion and platelet adhesion/activation on polyurethane ureas is related to hard segment content and composition, J. Biomater. Sci. Polym. Ed (6) (1994) 497–510.
[53] A. Butt, N.B. Lucchiari, D. Royhman, M.J. Runa, M.T. Mathew, C. Sukotjo, C.G. Takoudis, Design, development, and testing of a compact Tribocorrosion apparatus for biomedical applications, J. Bio-and Tribo-Corrosion. 1 (2014) 4, https://doi.org/10.1007/s40735-014-0004-6.
[54] T.R. Green, J. Fisher, M. Stone, B.M. Wroblewski, E. Ingham, Polyethylene particles of a "critical size" are necessary for the induction of cytokines by macrophages in vitro, Biomaterials. 19 (1998) 2297–2302, https://doi.org/10.1016/S0142-9612(98)00140-9.
[55] I. Voronov, J.P. Santerre, A. Hinek, J.W. Callahan, J. Sandhu, E.L. Boynton, Macrophage phagocytosis of polyethylene particulate in vitro, J. Biomed. Mater. Res. 39 (1997) 40–51, https://doi.org/10.1002/(SICI)1097-4636(199801)39:1<40::AID-JBM6>3.0.CO;2-I.
[56] B.T. Perez-Maceda, M.E. López-Fernández, I. Díaz, A. Kavanaugh, F. Billi, M.L. Escudero, M.C. García-Alonso, R.M. Lozano, Macrophage biocompatibility of CoCr wear particles produced under polarization in hyaluronic acid aqueous solution, Materials (Basel) 11 (2018), https://doi.org/10.3390/ma11050756.
[57] K.M. Shah, J.M. Wilkinson, A. Gartland, Cobalt and chromium exposure affects osteoblast function and impairs the mineralization of prosthesis surfaces in vitro, J. Orthop. Res. 33 (2015) 1663–1670, https://doi.org/10.1002/jor.22932.
[58] M.M. Sava, B. Munteanu, E. Renault, Y. Berthier, A.M. Trunfio-Sfarghiu, Tribological analysis of UHMWPE tibial implants in unicompartmental knee replacements: from retrieved to in vitro studies, Biotribology. 13 (2018) 1–15, https://doi.org/10.1016/j.biotri.2017.11.001.
[59] Y. Yan, A. Neville, J. Hesketh, D. Dowson, Real-time corrosion measurements to assess biotribocorrosion mechanisms with a hip simulator, Tribol. Int. 63 (2013) 115–122, https://doi.org/10.1016/j.triboint.2012.08.006.
[60] E.T. Skyttä, H. Koivu, A. Eskelinen, M. Ikävalko, P. Paavolainen, V. Remes, Total ankle replacement: a population-based study of 515 cases from the Finnish arthroplasty register, Acta Orthop. 81 (2010) 114–118, https://doi.org/10.3109/17453671003685459.
[61] Y. Yan, A. Neville, Bio-Tribocorrosion: Surface Interactions in Total Joint Replacement (TJR), in: Bio-Tribocorrosion Biomater, Woodhead Publishing Limited, Med. Implant, 2013, pp. 309–340, https://doi.org/10.1533/9780857098603.3.309.
[62] R.N. Stauffer, E.Y.S. Chao, R.C. Brewster, Force and motion analysis of the Normal, diseased, and prosthetic ankle joint, Clin. Orthop. Relat. Res. 127 (1977) 189–196.
[63] A. Seireg, R.J. Arvikar, The prediction of Musclular load sharing and joint forces in lower extremities during walking, J. Biomech. 8 (1975) 89–102.
[64] A.P.B.M. Saad, A. Syahrom, M.N. Harun, M.R.A. Kadir, Wear Prediction on Total Ankle Replacement Effect of Design Parameters, Springer, 2016.
[65] B. Reggiani, A. Leardini, F. Corazza, M. Taylor, Finite element analysis of a total ankle replacement during the stance phase of gait, J. Biomech. 39 (2006) 1435–1443, https://doi.org/10.1016/j.jbiomech.2005.04.010.
[66] B. Hintermann, Total Ankle Arthroplasty. Historical Overview, Current Concepts and Future Perspectives, SpringerWi, 2005.
[67] B. Ratner, A. Hoffman, F. Schoen, J. Lemons, Biomaterials Science. An Introduction to Materials in Medicine, Academic P, San Diego, 1996.
[68] L. Brizuela, A. Dayon, N. Doumerc, I. Ader, M. Golzio, J.C. Izard, Y. Hara, B. Malavaud, O. Cuvillier, The sphingosine kinase-1 survival pathway is a molecular target for the tumor-suppressive tea and wine polyphenols in prostate cancer, FASEB J. 24 (2010) 3882–3894, https://doi.org/10.1096/fj.10-160838.

[69] ASTM F1877-16, Standard Practice for Characterization of Particles, ASTM International, West Conshohocken, PA, 2016, https://doi.org/10.1520/F1877-16 www.astm.org.

[70] A.C. Vieira, A.R. Ribeiro, L.A. Rocha, J.P. Celis, Influence of pH and corrosion inhibitors on the tribocorrosion of titanium in artificial saliva, Wear. 261 (2006) 994–1001, https://doi.org/10.1016/j.wear.2006.03.031.

[71] A. Berradja, F. Bratu, L. Benea, G. Willems, J.P. Celis, Effect of sliding wear on tribocorrosion behaviour of stainless steels in a Ringer's solution, Wear. 261 (2006) 987–993, https://doi.org/10.1016/j.wear.2006.03.003.

[72] Y. Sun, R. Bailey, Improvement in tribocorrosion behavior of 304 stainless steel by surface mechanical attrition treatment, Surf. Coat. Technol. 253 (2014) 284–291, https://doi.org/10.1016/j.surfcoat.2014.05.057.

[73] Y. Yan, A. Neville, D. Dowson, Biotribocorrosion of CoCrMo orthopaedic implant materials — assessing the formation and effect of the biofilm, Tribol. Int. 40 (2007) 1492–1499, https://doi.org/10.1016/j.triboint.2007.02.019.

[74] I. Milošev, H.H. Strehblow, The composition of the surface passive film formed on CoCrMo alloy in simulated physiological solution, Electrochim. Acta 48 (2003) 2767–2774, https://doi.org/10.1016/S0013-4686(03)00396-7.

[75] V. Dalbert, Etude du comportement en tribocorrosion d'aciers inoxydables en milieu aqueux: évaluation de la synergie entre sollicitations mécaniques superficielles et réactions électrochimiques de surface, effet de la microstructure., INSA de Lyon, 2014.

[76] J.R. Goldberg, J.L. Gilbert, Electrochemical response of CoCrMo to high speed fracture of its metal oxide using an electrochemical stratch, J. Biomed. Mater. Res. 37 (1997) 421–431.

[77] M. Keddam, P. Ponthiaux, V. Vivier, Tribo-electrochemical impedance: a new technique for mechanistic study in tribocorrosion, Electrochim. Acta 124 (2014) 3–8, https://doi.org/10.1016/j.electacta.2013.08.186.

[78] A. Berradja, D. Déforge, R.P. Nogueira, P. Ponthiaux, F. Wenger, J.P. Celis, An electrochemical noise study of tribocorrosion processes of AISI 304 L in cl- and SO_4^{2-} media, J. Phys. D. Appl. Phys. 39 (2006) 3184–3192, https://doi.org/10.1088/0022-3727/39/15/S08.

[79] D. Sun, J.A. Wharton, R.J.K. Wood, Effects of proteins and pH on tribocorrosion performance of cast CoCrMo – a combined electrochemical and tribological study, Tribol. Mater. Surf. Interfaces. 2 (2008) 150–160, https://doi.org/10.1179/175158309X408315.

[80] M. Lyvers, D. Bijukumar, A. Moore, P. Saborio, D. Royhman, M. Wimmer, K. Shull, M.T. Mathew, Electrochemically induced tribolayer with molybdenum for hip implants: Tribocorrosion and biocompatibility study, Thin Solid Films 644 (2017) 82–91, https://doi.org/10.1016/j.tsf.2017.09.050.

[81] T. Hanawa, S. Hiromoto, K. Asami, Characterization of the surface oxide film of a co-Cr-Mo alloy after being located in quasi-biological environments using XPS, Appl. Surf. Sci. 183 (2001) 68–75, https://doi.org/10.1016/S0169-4332(01)00551-7.

[82] A.M. Trunfio-Sfarghiu, Y. Berthier, M.H. Meurisse, J.P. Rieu, Multiscale analysis of the tribological role of the molecular assemblies of synovial fluid. Case of a healthy joint and implants, Tribol. Int. 40 (2007) 1500–1515, https://doi.org/10.1016/j.triboint.2007.02.008.

[83] L. Vroman, A.L. Adams, M. Klings, Interactions among human blood proteins at interfaces, Fed. Proc. 30 (1971) 1494–1502.

[84] A. Smyth, J. Fisher, S. Suñer, C. Brockett, Influence of kinematics on the wear of a total ankle replacement, J. Biomech. 53 (2017) 105–110, https://doi.org/10.1016/j.jbiomech.2017.01.001.

[85] B. Kincaid, F. Gillard, D. Wentorf, O. Popoola, J. Bischoff, Gravimetric Wear Testing of a Fixed-Bearing Bicondylar Total Ankle Replacement, (2013).

[86] C.J. Bell, J. Fisher, Simulation of polyethylene Wear in ankle joint prostheses, J Biomed Mater Res B Appl Biomater 81B (2007) 162–167.

[87] T.S. Roukis, G.C. Berlet, C. Bibbo, C.F. Hyer, M.J. Penner, M. Wünschel, Primary and Revision Total Ankle Replacement, Springer, 2015.

[88] A. Kobayashi, Y. Minoda, Y. Kadoya, H. Ohashi, K. Takaoka, C.L. Saltzman, Ankle arthroplasties generate wear particles similar to knee arthroplasties, Clin. Orthop. Relat. Res. (2004) 69–72, https://doi.org/10.1097/01.blo.0000132182.54217.da.

[89] B. Hintermann, V. Valderrabano, Total ankle replacement, Foot Ankle Clin. 8 (2003) 375–405, https://doi.org/10.1016/S1083-7515(03)00015-9.

[90] I. Catelas, J.D. Bobyn, J.J. Medley, D.J. Zukor, A. Petit, O.L. Huk, The effect of digestion protocols on the isolation and characterization of metal– metal wear particles. II. Analysis of ion concentrations and particle composition, J. Biomed. Mater. Res. 55 (2001).

[91] W.G. Brodbeck, M.S. Shive, E. Colton, Y. Nakayama, T. Matsuda, J.M. Anderson, Influence of biomaterial surface chemistry on the apoptosis of adherent cells, J. Biomed. Mater. Res. A 55 (2001) 661–668.

[92] W.A. Soskolne, L. Sennerby, A. Wennerberg, The effect of titanium surface roughness on the adhesion of monocytes and their secretion of TNF- a and PGE 2, Clin. Oral Implants Res. 13 (2002) 86–93.

[93] D.B. Warheit, L.H. Hill, A.R. Brody, Surface morphology and correlated phagocytic capacity of pulmonary macrophages lavaged from the lungs of rats, Exp. Lung Res. 6 (1984) 71–82, https://doi.org/10.3109/01902148409087896.

[94] F.Y. McWhortera, T. Wanga, P. Nguyena, T. Chunga, W.F. Liu, Modulation of macrophage phenotype by cell shape, Proc. Natl. Acad. Sci. 110 (2013) 17253–17258.

[95] A.S. Shanbhag, J.J. Jacobs, J. Black, J.O. Galante, T.T. Glant, Macrophage/particle interactions: effect of size, composition and surface area, J. Biomed. Mater. Res. 28 (1994) 81–90, https://doi.org/10.1002/jbm.820280111.

[96] R. Shrivastava, R.K. Upreti, P.K. Seth, U.C. Chaturvedi, Effects of chromium on the immune system, FEMS Immunol. Med. Microbiol. 34 (2002) 1–7, https://doi.org/10.1111/j.1574-695X.2002.tb00596.x.

[97] C.H. Lohmann, Z. Schwartz, G. Köster, U. Jahn, G.H. Buchhorn, M.J. MacDougall, D. Casasola, Y. Liu, V.L. Sylvia, D.D. Dean, B.D. Boyan, Phagocytosis of wear debris by osteoblasts affects differentiation and local factor production in a manner dependent on particle composition, Biomaterials. 21 (2000) 551–561, https://doi.org/10.1016/S0142-9612(99)00211-2.

[98] J.L. Gilbert, L. Zarka, E. Chang, C.H. Thomas, The reduction half cell in biomaterials corrosion: oxygen diffusion profiles near and cell response to polarized titanium surfaces, J. Biomed. Mater. Res. 42 (1998) 321–330, https://doi.org/10.1002/(SICI)1097-4636(199811)42:2<321::AID-JBM18>3.0.CO;2-L.

[99] J.A. Stolwijk, C. Hartmann, P. Balani, S. Albermann, C.R. Keese, I. Giaever, J. Wegener, Impedance analysis of adherent cells after in situ electroporation: non-invasive monitoring during intracellular manipulations, Biosens. Bioelectron.s 26 (2011) 4720–4727, https://doi.org/10.1016/j.bios.2011.05.033.

[100] O.L. Huk, I. Catelas, F. Mwale, J. Antoniou, D.J. Zukor, A. Petit, Induction of apoptosis and necrosis by metal ions in vitro, J. Arthroplast. 19 (2004) 84–87, https://doi.org/10.1016/j.arth.2004.09.011.

[101] L.D. Dorr, R. Bloebaum, J. Emmanual, R. Meldrum, Histologic, biochemical, and ion analysis of tissue and fluids retrieved during total hip arthroplasty, Clin. Orthop. Relat. Res. 261 (1990) 82–95, https://doi.org/10.1097/00003086-199012000-00010.

[102] M. Böhler, F. Kanz, B. Schwarz, I. Steffan, A. Walter, H. Plenk Jr., K. Knahr, Adverse tissue reactions to wear particles from co-alloy articulations, increased by alumina-blasting particle contamination from cementless Ti-based total hip implants, J. Bone Jt. Surg. 84 (2002) 128–136, https://doi.org/10.1302/0301-620X.84B1.11324.

[103] Y. Wang, Y. Yan, Y. Su, L. Qiao, Release of metal ions from nano CoCrMo wear debris generated from tribo-corrosion processes in artificial hip implants, J. Mech. Behav. Biomed. Mater. 68 (2017) 124–133, https://doi.org/10.1016/j.jmbbm.2017.01.041.

[104] J.B. Matthews, A.A. Besong, T.R. Green, M.H. Stone, B.M. Wroblewski, J. Fisher, E. Ingham, Evaluation of the response of primary human peripheral blood mononuclear phagocytes to challenge with in vitro generated clinically relevant UHMWPE particles of known size and dose, J. Biomed. Mater. Res. 52 (2000) 296–307, https://doi.org/10.1002/1097-4636(200011)52:2<296::AID-JBM8>3.0.CO;2-9.

[105] M. Endo, J.L. Tipper, D.C. Barton, M.H. Stone, E. Ingham, J. Fisher, Comparison of wear, wear debris and functional biological activity of moderately crosslinked and non-crosslinked polyethylenes in hip prostheses, Proc. Inst. Mech. Eng. Part H J. Eng. Med. 216 (2002) 111–122, https://doi.org/10.1243/0954411021536333.

[106] P.F. Doorn, P.A. Campbell, J. Worrall, P.D. Benya, H.A. Mckellop, H.C. Amstutz, Metal wear particle characterization from metal on metal total hip replacements : transmission electron microscopy study of periprosthetic tissues and isolated particles, (1998), J Biomed Mater Res 42 (1) (1998) 103–111.

[107] F. Billi, P. Benya, E. Ebramzadeh, P. Campbell, F. Chan, H.A. McKellop, Metal wear particles: what we know, what we do not know, and why, SAS J. 3 (2009) 133–142, https://doi.org/10.1016/j.esas.2009.11.006.

[108] S. Yang, W. Ren, Y. Park, A. Sieving, S. Hsu, S. Nasser, P.H. Wooley, Diverse cellular and apoptotic responses to variant shapes of UHMWPE particles in a murine model of inflammation, Biomaterials 23 (2002) 3535–3543.

[109] A. Sieving, B. Wu, L. Mayton, S. Nasser, P.H. Wooley, Morphological characteristics of total joint arthroplasty-derived ultra-high molecular weight polyethylene (UHMWPE) wear debris that provoke, J. Biomed. Mater. Res. A 64 (2003) 457–464.

[110] N. Ishiguro, T. Kojima, T. Ito, S. Saga, H. Anma, K. Kurokouchi, Y. Iwahori, T. Iwase, H. Iwata, Macrophage activation and migration in interface tissue around loosening total hip arthroplasty components, J. Biomed. Mater. Res. 35 (1997) 399–406, https://doi.org/10.1002/(SICI)1097-4636(19970605)35:3<399::AID-JBM14>3.0.CO;2-A.

[111] E. Ingham, J. Fisher, Biological reactions to wear debris in total joint replacement, Inst. Mech. Eng. Part H J. Eng. Med. (2000) 21–37, https://doi.org/10.1243/0954411001535219.

[112] S. Gupta, J.K. Ellington, M.S. Myerson, Management of specific complications after revision total ankle replacement, Semin. Arthroplast. 21 (2010) 310–319, https://doi.org/10.1053/j.sart.2010.09.013.

[113] R. Meldrum, B. Roy, D. Lawrence, Metal ion concentrations in retrieved polyethylene total hip inserts and implications for artifactually high readings in tissue, J. Biomed. Mater. Res. 27 (1993) 1349–1355.

[114] C. Gray, D. Zicha, John M. Davis (Ed.), Microscopy of living cells, 2011, pp. 61–90, , https://doi.org/10.1002/9780470669815 Anim. Cell Cult. Essent. Methods.

[115] I. Garcia, D. Drees, J. Celis, Corrosion-wear of passivating materials in sliding contacts based on a concept of active wear track area, Wear 249 (2001) 452–460.

[116] M.T. Mathew, C. Nagelli, R. Pourzal, A. Fischer, M.P. Laurent, J.J. Jacobs, M.A. Wimmer, Tribolayer formation in a metal-on-metal (MoM) hip joint: an electrochemical investigation, J. Mech. Behav. Biomed. Mater. 29 (2014) 199–212, https://doi.org/10.1016/j.jmbbm.2013.08.018.

[117] J. Hesketh, M. Ward, D. Dowson, A. Neville, The composition of tribofilms produced on metal-on-metal hip bearings, Biomaterials. 35 (2014) 2113–2119, https://doi.org/10.1016/j.biomaterials.2013.11.065.

[118] J.J. Ryu, P.S. Hrotriya, Synergistic Mechanisms of Bio-Tribocorrosion in Medical Implants, in: Bio-Tribocorrosion Biomater, Woodhead Publishing Limited, Med.

Implant, 2013, pp. 25–44, https://doi.org/10.1533/9780857098603.1.25.
[119] A. Impergre, B. Ter-Ovanessian, C. Der Loughian, B. Normand, Systemic strategy for biocompatibility assessments of metallic biomaterials: representativeness of cell culture medium, Electrochim. Acta 283 (2018) 1017–1027, https://doi.org/10.1016/j.electacta.2018.06.196.
[120] T. Veselack, G. Aldebert, A.-M. Trunfio-Sfarghiu, T. Schmid, M. Laurent, M. Wimmer, Phospholipid vesicles in Media for Tribological Studies against live cartilage, Lubricants. 6 (2018) 19, https://doi.org/10.3390/lubricants6010019.
[121] A. Dalal, V. Pawar, K. Mcallister, C. Weaver, N.J. Hallab, Orthopedic implant cobalt-alloy particles produce greater toxicity and inflammatory cytokines than titanium alloy and zirconium alloy-based particles in vitro, in human osteoblasts, fibroblasts, and macrophages, J Biomed Mater Res Part A 100A (2012) 2147–2158, https://doi.org/10.1002/jbm.a.34122.